Rhodium(III) and Iridium(III) Complexes of a Neopentyl-Substituted PNP Pincer Ligand that Feature Agostic Interactions

Smart, Jennifer E.; Prokes, Ivan; Leforestier, Baptiste; Chaplin, Adrian B.

How to cite

SMART, Jennifer E. et al. Rhodium(III) and Iridium(III) Complexes of a Neopentyl-Substituted PNP Pincer Ligand that Feature Agostic Interactions. In: Organometallics, 2024, vol. 43, n° 10, p. 1143–1154. doi: 10.1021/acs.organomet.4c00081

This publication URL: https://archive-ouverte.unige.ch/unige:184214
Publication DOI: 10.1021/acs.organomet.4c00081

ORGANOMETALLICS

pubs.acs.org/Organometallics

Article

Rhodium(III) and Iridium(III) Complexes of a Neopentyl-Substituted PNP Pincer Ligand that Feature Agostic Interactions

Jennifer E. Smart, Ivan Prokes, Baptiste Leforestier,* and Adrian B. Chaplin*

Cite This: *Organometallics* 2024, 43, 1143−1154

Read Online

ACCESS | Metrics & More | Article Recommendations | Supporting Information

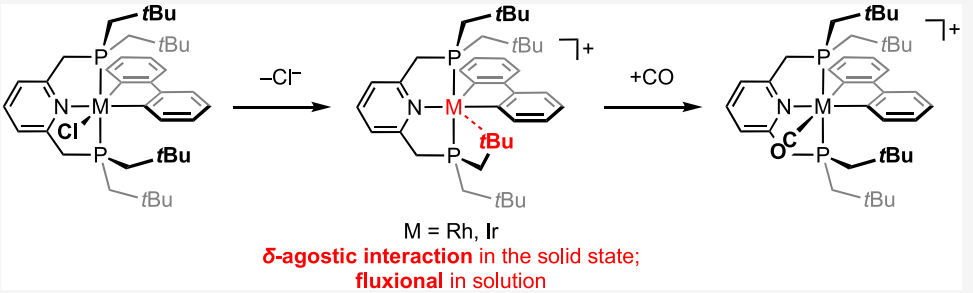

ABSTRACT: The synthesis and characterization of five-coordinate rhodium(III) and iridium(III) complexes of the form [M(PNP-Np)(biph)][BAr^F_4] are described, where PNP-Np is the neopentyl-substituted pincer ligand 2,6-(Np_2PCH_2)$_2C_5H_3N$ (Np = CH_2tBu), biph = 2,2′-biphenyl, and Ar^F = 3,5-(CF_3)$_2C_6H_3$. These complexes are notable for the adoption of δ-agostic interactions in the solid state, as evidenced by X-ray crystallography (50−150 K) and ATR-IR spectroscopy, but are structurally dynamic in solution, exhibiting pseudorotation of the biph ligand on the ^{1}H NMR time scale (185−308 K). The strength of the agostic interactions is discussed with reference to the known *tert*-butyl-substituted analogues [M(PNP-*t*Bu)(biph)][BAr^F_4], probed by reaction with carbon monoxide, and quantified computationally through NBO analysis, from which the conclusion is that 3-center−2-electron bonding increases in the order M = Ir > Rh (cf. 1.5× greater perturbation energy) and pincer ligand = PNP-Np > PNP-*t*Bu (cf. 3.3× greater perturbation energy).

1. INTRODUCTION

The coordination chemistry of aliphatic C−H bonds remains an important topic in organometallic chemistry.[1] Adoption of 3-center−2-electron (3c−2e) M−H−C interactions can help stabilize otherwise reactive low-coordinate metal complexes and is implicated in the mechanism of concerted C−H bond oxidative addition reactions to low-valent transition metals.[2] As a consequence of the weakly interacting nature of C−H bonds, well-defined examples of M−H−C bonding are almost exclusively limited to intramolecular systems that are stabilized by the chelate effect. Such intramolecular interactions are termed "agostic" and typified by M−H−C contacts up to ∼3 Å.[3] The characterization of σ-alkane complexes is significantly more experimentally demanding but has been achieved in solution using time-resolved spectroscopic methods at low temperature and, recently, in the solid state by X-ray crystallography through application of single-crystal to single-crystal transformations.[4]

With respect to the precious metals rhodium and iridium, numerous complexes with agostic interactions can be identified in the literature, with >150 deposited in the CSD (v. 5.43). M(III) systems featuring agostic interactions opposite to a high trans-influence hydride, aryl, or alkyl ligand are common, but homologous series are rare.[5] Series of this nature are of interest to gauge an understanding of the effect of the metal alongside subtle variations of the ligand composition on the constituent agostic interactions. In this regard, low-coordinate M(III) complexes of 2,2′-biphenyl (biph) **A**−**E** are noteworthy (Figure 1), with the majority resulting from work carried out in our group over the past 6 years.[6−10] Most pertinent to the study described herein, this set includes formally five-coordinate pincer complexes [M(PNP-*t*Bu)(biph)][BAr^F_4] (M = Rh, **1**; Ir, **2**; PNP-*t*Bu = 2,6-(tBu_2PCH_2)$_2C_5H_3N$; Ar^F = 3,5-(CF_3)$_2C_6H_3$).[6] These complexes are characterized by time-averaged C_{2v} symmetry in solution as a result of facile pseudorotation of the biph ligand on the ^{1}H NMR time scale ($\Delta G^{\ddagger}$ = 56 ± 1 kJ mol^{-1}, **1**; 62 ± 1 kJ mol^{-1}, **2**) but adopt square pyramidal geometries in the solid state which are stabilized by weak γ-agostic interactions (M−H−C ∼ 3.0 Å).

Reasoning that more flexible phosphine substituents would enable adoption of stronger, more persistent δ-agostic interactions with the metal center, we herein report on the

Received: February 28, 2024
Revised: April 12, 2024
Accepted: April 17, 2024
Published: May 3, 2024

https://doi.org/10.1021/acs.organomet.4c00081
Organometallics 2024, 43, 1143−1154

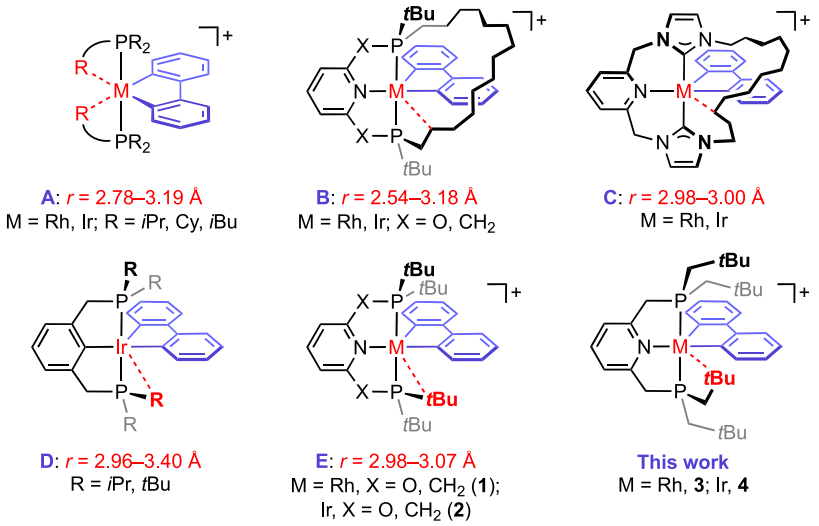

Figure 1. Low-coordinate M^{III}(biph) complexes stabilized by agostic interactions.

synthesis, characterization, and reactivity of five-coordinate pincer complexes [M(PNP-Np)(biph)][BAr^F_4] (M = Rh, **3**; Ir, **4**; Figure 1), where PNP-Np is a neopentyl-substituted pincer ligand developed by Yamashita, Nozaki, and co-workers (PNP-Np = 2,6-(Np_2PCH_2)$_2C_5H_3N$; Np = CH_2tBu).[11]

2. RESULTS AND DISCUSSION

2.1. Ligand Synthesis and M(I) Carbonyl Derivatives.

Neopentyl-substituted pincer ligand PNP-Np was prepared using the reported procedure, involving treatment of doubly deprotonated 2,6-lutidine with di(neopentyl)chlorophosphine (Scheme 1).[11] Whilst the pincer ligand was obtained as the major product following this method, we find that borane protection and purification by column chromatography is the most expedient route to obtain pure material. Deprotection of the corresponding phosphine-borane adduct (δ_{31P} 10.7) was achieved by heating with diethylamine and pure PNP-Np (δ_{31P} −39.9) obtained upon removal of volatiles under high vacuum (including amine-borane).

Scheme 1. Preparation and Purification of PNP-Np[a]

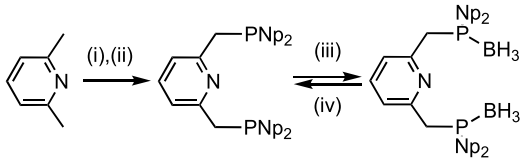

[a]Reagents and conditions: (i) *n*BuLi, TMEDA; Et_2O, 0 °C → RT, 21 h; (ii) Np_2PCl; Et_2O, −78 °C → 30 °C, 92 h; (iii) $H_3B{\cdot}SMe_2$; THF, −78 °C → RT, 0.5 h (65%, 3 steps); (iv) Et_2NH; 80 °C, 48 h (84%).

To quantify the relative donor strength of the PNP-Np ligand, M(I) carbonyl derivatives were prepared for analysis by IR spectroscopy (Scheme 2).[12,13] The new rhodium variant **5** was obtained in good yield by reaction of $[Rh(CO)_2Cl]_2$ with PNP-Np in fluorobenzene, using Na[BAr^F_4] as the halide abstracting agent, and fully characterized in solution (C_{2v} symmetric; δ_{31P} 17.4, $^1J_{RhP}$ = 121 Hz) and the solid state (Figure 2A).[14] The iridium carbonyl complex [Ir(PNP-Np)(CO)]BF_4 has been reported previously,[11] and [BAr^F_4]$^-$ analogue **6** was prepared using a variation of the reported two-step procedure, employing [Ir(COD)$_2$][BAr^F_4] (COD = 1,5-cyclooctadiene) as the metal

Scheme 2. Preparation of M^I(CO) Complexes[a]

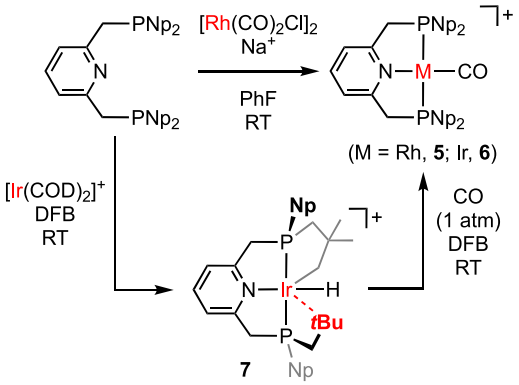

[a][BAr^F_4]$^-$ counterions omitted.

precursor and 1,2-difluorobenzene (DFB) as the solvent. The intermediate cyclometalated iridium(III) hydride **7** involved in this procedure was isolated and fully characterized. The spectroscopic characteristics are consistent with the literature (C_1 symmetric; δ_{1H} −16.81, $^2J_{PH}$ = 12 Hz; δ_{31P} 18.5, 28.5, $^2J_{PP}$ = 316 Hz) and in this case the salt is amenable to structural characterization by X-ray diffraction (previously trapped out as a coordinatively saturated acetonitrile adduct,[11] Figure 2B). In the solid state, **7** adopts a square pyramidal metal geometry which is stabilized by a δ-agostic interaction (Ir1−C30 = 2.759(10) Å) *trans* to the cyclometalated neopentyl substituent (Ir1−C40 = 2.145(8) Å). These bonding modes are readily apparent from the metal−carbon metrics and vindicated by the relative compression of the Ir1−P2−C28 (110.2(4)°) and Ir1−P3−C38 (104.2(3)°) angles compared to those of free phosphine substituents (ca. 130°). Treatment of **7** with CO (1 atm) afforded **6** in acceptable purity for the desired IR study (δ_{31P} 13.6).

The carbonyl-stretching bands of **5** and **6** were determined by IR analysis in CH_2Cl_2 solution at room temperature and compared to values established for the PNP-*t*Bu homologues under these conditions (Table 1).[6] The neopentyl-substituted systems exhibit ν(CO) frequencies that are blue-shifted by 14 cm^{-1}, indicating that PNP-Np is an appreciably weaker net donor than PNP-*t*Bu. This conclusion is fully in line with

https://doi.org/10.1021/acs.organomet.4c00081
Organometallics 2024, 43, 1143−1154

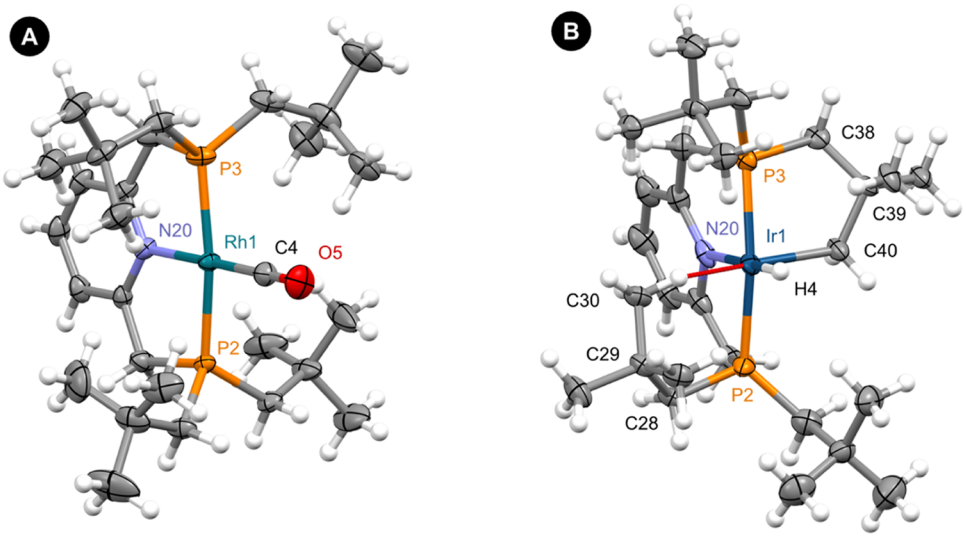

Figure 2. Solid-state structures of (A) rhodium(I) carbonyl **5** and (B) cyclometalated iridium(III) hydride **7**; one of the two unique cations shown for **5** (Z' = 2), ellipsoids drawn at 30% probability, and anions omitted for clarity. Selected bond lengths (Å) and angles (deg): **5**, Rh1−P2, 2.2915(9); Rh1−P3, 2.2930(10); Rh1−N20, 2.096(3); Rh1−C4, 1.845(4); C4−O5, 1.133(5); P2−Rh1−P3, 168.99(4); N20−Rh1−C4, 179.03(16); omitted cation, Rh1A−P2A, 2.2933(9); Rh1A−P3A, 2.2969(9); Rh1A−N20A, 2.095(3); Rh1A−C4A, 1.841(4); C4A−O5A, 1.142(5); P2A−Rh1A−P3A, 168.74(4); N20A−Rh1A−C4A, 177.72(13); **7**, Ir1−P2, 2.271(2); Ir1−P3, 2.271(2); Ir1−N20, 2.173(7); Ir1−C40, 2.145(8); Ir1−H4, 1.5 (restrained); Ir1−C30, 2.759(10), P2−Ir1−P3, 162.71(8); N20−Ir1−C40, 89.5(3); C40−Ir1−C30, 173.0(3).

Table 1. Carbonyl Stretching Frequencies of $[M(PNP\text{-}R)(CO)]^+$ in CH_2Cl_2

complex	ν(CO) (cm^{-1})
$[Rh(PNP\text{-}t\text{Bu})(CO)][BAr^F{}_4]$	1990
$[Rh(PNP\text{-}Np)(CO)][BAr^F{}_4]$ **5**	2004
$[Ir(PNP\text{-}t\text{Bu})(CO)][BAr^F{}_4]$	1977
$[Ir(PNP\text{-}Np)(CO)][BAr^F{}_4]$ **6**	1991

expectation for the change in P-substituents from tertiary to primary alkyl groups. For instance, the Tolman electronic parameters of $PtBu_3$ and PEt_3 are 2056 and 2062 cm^{-1}, respectively.[15]

2.2. Preparation of M(III) Derivatives. Coordinatively saturated rhodium(III) and iridium(III) biph complexes [M(PNP-Np)(biph)Cl] (M = Rh, **8**; Ir, **9**) were prepared by ligand substitution reactions of [Rh(biph)(dtbpm)Cl] (dtbpm = bis(di-*tert*-butylphosphino)methane) and $[Ir(biph)(COD)Cl]_2$ with PNP-Np in fluorobenzene at elevated temperature (Scheme 3).[16] These new complexes were isolated in >60% yield and structurally corroborated in solution and the solid state. Analysis by NMR spectroscopy in CD_2Cl_2 indicates the adoption of C_s symmetry in solution, with **8** and **9** presenting single ^{31}P NMR resonances at δ 26.2 ($^1J_{RhP}$ = 109 Hz) and 0.6, respectively. This symmetry is manifested in the ^{1}H NMR spectra of the complexes by 2× inequivalent Np groups, diastereotopic pyCH_2 resonances, and 8× distinct environments for the biph ligand, which were assigned with the aid of 2D NMR experiments. The most shielded *t*Bu groups are assigned to those straddling the biph ligand, and the proximity to the aromatic rings is readily apparent from inspection of the isomorphic crystal structures of **8** and **9** (Figure 3A), which are otherwise unremarkable.

Generation of the target coordinatively unsaturated complexes [M(PNP-Np)(biph)][$BAr^F{}_4$] (M = Rh, **3**; Ir, **4**) was achieved by treatment of **8** and **9** with Na[$BAr^F{}_4$] in fluorobenzene at room temperature (Scheme 3) and verified *in situ* by perturbation of the ^{31}P NMR resonances, which are shifted to δ 23.8 ($^1J_{RhP}$ = 111 Hz) and 11.2, respectively, and the onset of fluxional behavior on the ^{1}H NMR time scale at 298 K. The complexes were subsequently isolated as analytically pure materials in >80% yield and extensively characterized in solution and the solid state as discussed below, focusing on the presence and features of the supporting agostic interactions.

2.3. Variable-Temperature Characterization and Analysis of Agostic Interactions in 3 and 4. Single crystals of **3** and **4** suitable for analysis by X-ray diffraction were grown by recrystallization from $SiMe_4$ diffusion into CH_2Cl_2 or CH_2Cl_2/

Scheme 3. Preparation of M^{III}(biph) Complexes[a]

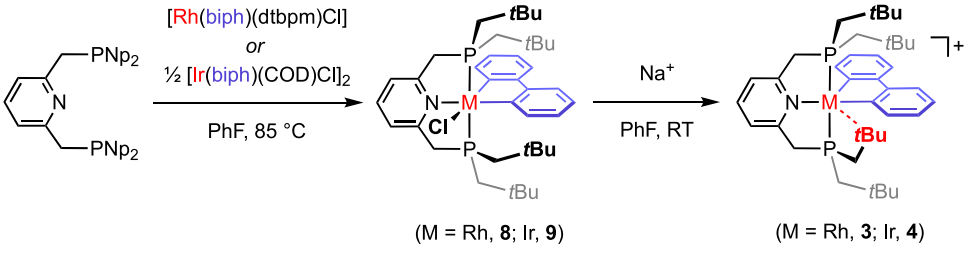

(M = Rh, **8**; Ir, **9**) (M = Rh, **3**; Ir, **4**)

[a] $[BAr^F{}_4]^-$ counterions omitted.

https://doi.org/10.1021/acs.organomet.4c00081
Organometallics 2024, 43, 1143−1154

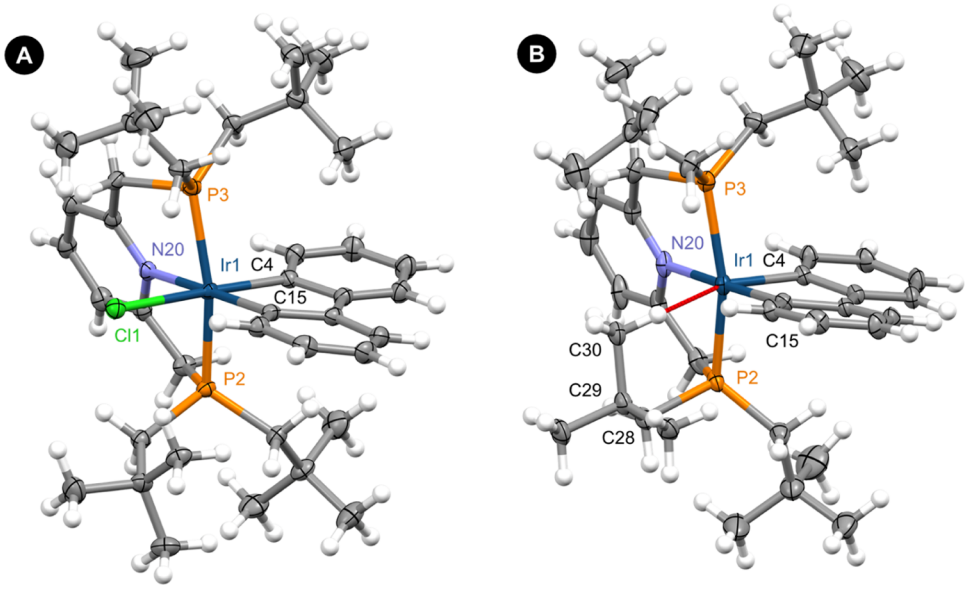

Figure 3. Solid-state structures of (A) coordinatively saturated iridium(III) complex **9** and (B) unsaturated iridium(III) complex **4** recorded at 150 K; ellipsoids drawn at 50 and 30% probability, respectively, with solvents ($SiMe_4$ and CH_2Cl_2 in **4**) and anions omitted for clarity. Selected bond lengths (Å) and angles (deg) for **8** and **9**, which are isomorphous: **8**, Rh1−P2, 2.3155(6); Rh1−P3, 2.3352(6); Rh1−N20, 2.150(2); Rh1−Cl1, 2.5021(6); Rh1−C4, 2.027(3); Rh1−C15, 2.034(2); P2−Rh1−P3, 164.33(2); N20−Rh1−C15, 176.41(10); Cl1−Rh1−C4, 176.83(7); **9**, Ir1−P2, 2.3166(6); Ir1−P3, 2.3275(6); Ir1−N20, 2.145(2); Ir1−Cl1, 2.4968(6); Ir1−C4, 2.040(2); Ir1−C15, 2.053(2); P2−Ir1−P3, 164.03(2); N20−Ir1−C15, 176.59(9); Cl1−Ir1−C4, 176.36(7).

Table 2. Selected Bond Lengths (Å), Angles (deg), and Unit Cell Volumes (Å^3) for [M(PNP-Np)(biph)][BAr^F_4][a]

	M = Rh, **3**			M = Ir, **4**		
T	50 K	100 K	150 K	50 K	100 K	150 K
M1−P2	2.2802(12)	2.2822(6)	2.2842(7)	2.2922(12)	2.2945(10)	2.2944(10)
M1−P3	2.3260(13)	2.3331(7)	2.3335(7)	2.3239(12)	2.3245(11)	2.3256(10)
M1−N20	2.152(4)	2.156(2)	2.157(2)	2.146(4)	2.150(3)	2.149(3)
M1−C4	2.016(3)	2.012(2)	2.012(2)	2.025(4)	2.022(4)	2.025(4)
M1−C15	2.037(4)	2.035(2)	2.034(3)	2.050(4)	2.056(4)	2.056(3)
M1−C30	2.890(4)	2.887(3)	2.906(3)	2.822(5)	2.831(4)	2.842(4)
P2−M1−P3	163.17(4)	163.33(2)	163.42(2)	163.22(4)	163.25(4)	163.24(4)
N20−M1−C15	177.02(15)	177.16(8)	177.32(9)	176.44(16)	176.50(14)	176.57(13)
M1−P2−C28	110.71(17)	110.25(9)	110.54(10)	110.40(17)	110.35(15)	110.47(14)
P2−C28−C29	116.0(3)	116.23(18)	116.2(2)	115.2(3)	115.3(3)	115.3(3)
volume	7979.97(12)	8038.95(6)	8140.90(6)	7971.38(8)	8041.82(8)	8133.38(8)

[a]Labeling as indicated in Figure 3B.

n-hexane solutions at −30 °C and are isomorphous (monoclinic $P2_1/n$). Mindful of previous variable-temperature studies on M^{III}(biph) complexes,[6,8] crystallographic data were collected for **3** and **4** at 50, 100, and 150 K. The solid-state structure of **4** at 150 K is presented in Figure 3B, and the most pertinent metrics are provided in Table 2.

The complexes adopt C_1-symmetric pseudo square pyramidal metal geometries with near-ideal N20−M1−C15 but distinctly obtuse P2−M1−P3 angles (∼163°) in accordance with the structures of PNP-*t*Bu analogues **1** and **2**.[6] The *t*Bu group of one the Np-substituents is canted toward the vacant coordination site and characterized by M1−H−C30 contacts of 2.822(5)−2.906(3) Å and relatively compressed M1−P2−C28 angles of (∼111°) compared to those of free phosphine substituents. These features mark out the presence of *δ*-agostic interactions in **3**/**4**,[3] and the metal−carbon contacts suggest that they are stronger than the respective *γ*-agostic interactions observed in **1**/**2** (M−H−C ∼ 3.0 Å). Consistent with this suggestion, the electronically correlated M1−C4 bonds *trans* to the agostic interaction are significantly longer in **3**/**4** (2.012(2)/2.025(4) Å @150 K) compared to those in **1**/**2** (1.988(2)/2.001(2) Å @ 150 K). In line with periodic trends, more pronounced 3c−2e bonding is apparent in the third row congener with ∼0.06 Å shorter M1−H−C30 distances measured across the temperature range.[17] While marginal, it is interesting to note that there is a statistically significant contraction of these contacts on cooling from 150 to 50 K, Δr = +0.016 ± 0.015 Å for **3** and +0.020 ± 0.019 Å for **4**. The contraction correlates with a ∼160 Å^3 (2%) decrease in the unit cell volume, and similar trends have been analyzed in detail for **A** and can be deduced from the reported variable-temperature data for **1** and **2**, where M−H−C contractions from 3.057(4) to 3.009(2) Å (Δr = +0.048 ± 0.013 Å) and 3.039(5) to 2.976(3) Å (Δr = +0.063 ± 0.017 Å) occur on cooling from 200 to 75 K, respectively.[6,8] The conformation of the pincer ligand backbone in **1** and **2** is dynamic in the solid

https://doi.org/10.1021/acs.organomet.4c00081
Organometallics 2024, 43, 1143−1154

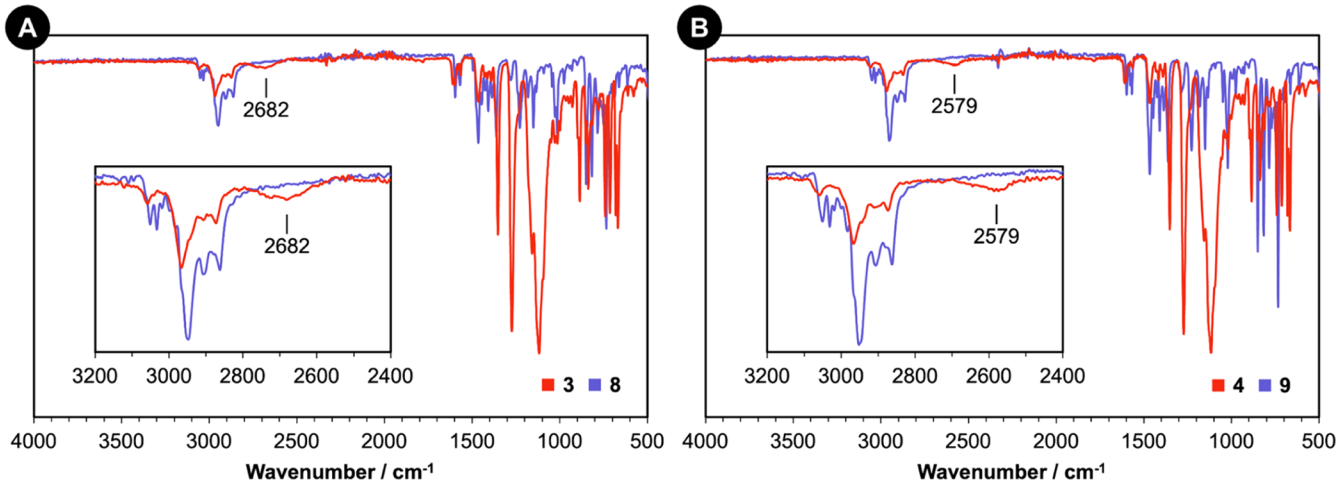

Figure 4. ATR-IR spectra of (A) Rh^{III}(biph) complexes **3** and **8** and (B) Ir^{III}(biph) complexes **4** and **9**.

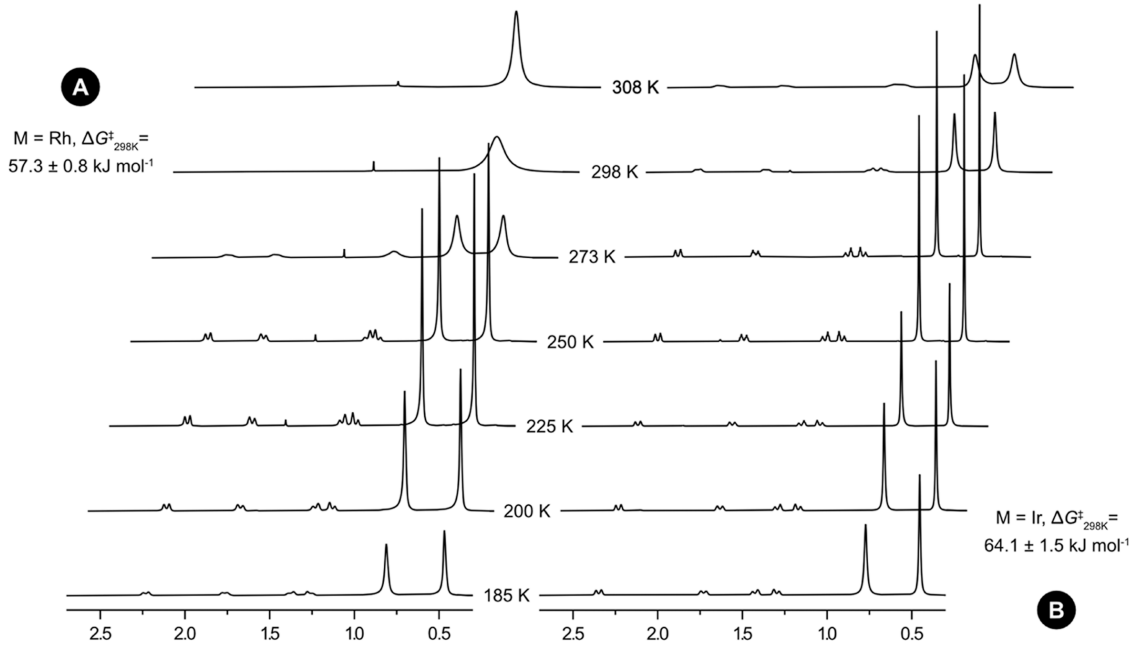

Figure 5. ^{1}H NMR spectra of (A) Rh^{III}(biph) complex **3** and (B) Ir^{III}(biph) complex **4** showing the effect of temperature on the Np resonances (CD_2Cl_2, 500 MHz).

state, but there is no evidence of equivalent disorder in **3** and **4** at the temperatures measured.[6]

Analysis of **3** and **4** by attenuated total reflection-infrared (ATR-IR) spectroscopy provides further support for the presence of substantial agostic interactions in the solid state.[3,18] The spectra show broad, reduced frequency ν(C−H) stretching bands centered at 2682 and 2579 cm^{-1}, respectively, that are not present in the parent chloro derivatives **8** and **9** (Figure 4). These spectroscopic markers were not resolved for the PNP-*t*Bu analogues **1** and **2** but are of similar frequency to those reported for macrocyclic M^{III}(biph) complexes **C** (Figure 1; M = Rh, 2682 cm^{-1}; M = Ir, 2571 cm^{-1}),[7] which adopt persistent agostic interactions in solution. The relative red shifts of the ν(C−H) stretching bands are also consistent with stronger Ir−H−C compared to Rh−H−C interactions inferred geometrically from the crystal structures of **3** and **4**.

In CD_2Cl_2 solution, **3** and **4** exhibit fluxional structures with varying degrees of decoalescence from time-averaged C_{2v} to C_s symmetry evident from ^{1}H NMR spectra collected from 308 down to 185 K at 500 MHz. Both symmetries are incompatible with adoption of persistent agostic interactions, and the principal dynamic is attributed to pseudorotation of the biph ligand on the ^{1}H NMR time scale ($C_s \rightleftharpoons C_s \rightarrow C_{2v}$; Figure S50). This process is considerably more facile for rhodium congener **3**, where coalescence is reached within the upper-temperature limit of the solvent, as evidenced by collection of a broadened C_{2v} symmetric ^{1}H NMR spectrum at 308 K (Figure 5). Sharp C_s-symmetric spectra of **3** and **4** were obtained upon cooling to 250 and 273 K, respectively, and simulation of variable-temperature ^{1}H NMR data using gNMR enabled activation parameters associated with the biph pseudorotation to be determined for both complexes (**3**, $\Delta G_{298\,K}^{\ddagger} = 57.3 \pm 0.8$ kJ mol^{-1}; **4**, $\Delta G_{298\,K}^{\ddagger} = 64.1 \pm 1.5$ kJ mol^{-1}).[19] Whilst the trend is to higher values, these activation barriers are not statistically different from those reported for **1** (56 ± 1 kJ mol^{-1}) and **2** (62 ± 1 kJ mol^{-1}), respectively, where steric buttressing between the P-substituents

https://doi.org/10.1021/acs.organomet.4c00081
Organometallics 2024, 43, 1143−1154

and the biph ligand was identified as a major contributing factor.[6] Thus, these data are consistent with adoption of stronger agostic interactions in **3** and **4** compared to **1** and **2**, respectively, due to the considerably less sterically imposing nature of the Np-substituents compared to the *t*Bu-substituents. Viewed another way, pseudorotation is hindered by ground state stabilization in the former and transition state destabilization in the latter.

With respect to the adoption of agostic interactions in solution, it is interesting to note that the onset of further decoalesence is apparent at low temperatures from line broadening of the most deshielded *t*Bu resonances of the 2× inequivalent Np-substituents of **3** and **4** in the ^{1}H NMR spectra (Figure 5). These signals are assigned to the *t*Bu group proximal to the vacant coordination site based on comparison to **8**/**9** and NOESY experiments carried out at 200 K, with an appreciable NOE interaction with the 6-biph signal detected. We tentatively attribute this low energy process to dynamic interconversion between C_1 conformations on the ^{1}H NMR time scale, where agostic interactions are formed with Np-substituents of opposing phosphine donors ($C_1 \rightleftharpoons C_1 \rightarrow C_s$; Figure S50). This phenomenon is most pronounced for **4**, congruent with the relative strength of the M−H−C interactions inferred in the solid state.

2.4. Computational Analysis of Agostic Interactions in 3 and 4. To further scrutinize the agostic interactions, the cations of **3** and **4** were analyzed using DFT-based computational methods at the ωB97X-D4/def2-TZVP level of theory.[20] The optimized gas-phase structures are characterized by a slight relaxation in geometry compared to the crystal structures, but the trends in metal-based bond lengths and bond angles are well reproduced. Most notably, whilst the agostic interactions are contracted by ∼0.1 Å *in silico*, the observation of Rh−H−C > Ir−H−C was verified computationally. The relative strength of the 3c−2e bonding inferred from this metric was substantiated by relaxed potential energy scans, in which elongation of the M−H−C bond was found to have a greater energetic penalty for the M = Ir ($\Delta E_{1\ Å}$ = +8.2 kcal mol^{-1}) compared to Rh ($\Delta E_{1\ Å}$ = +6.7 kcal mol^{-1}) congener.

The electronic structures of **3** and **4** have been examined using the Natural Bond Orbital (NBO) approach[21] and contrasted to **1** and **2** optimized at the same level of theory (Table 3). From the second-order perturbation analysis, agostic interactions with shorter M−H−C distances are associated with increased stabilization energies (both σ-donation and π-back-donation), decreased occupancy of the σ_{CH} NBOs, and increased occupancy of the σ^*_{CH} NBOs. For complexes of the form [M(PNP-R)(biph)]$^+$, these results show that stronger agostic interactions are formed for M = Ir compared to Rh (**2** vs **1** and **4** vs **3**; cf. 1.5× greater perturbation energies) and most significantly for R = Np compared to *t*Bu (viz. **1** vs **3** and **2** vs **4**; cf. 3.3× greater perturbation energies). With respect to the pincer ligand, closer inspection of the optimized structures suggests that the flexible Np-substituents enable a more favorable interaction between the C−H bond and frontier molecular orbitals of the metal, as evidenced not only by shorter M−H−C distances but also by more obtuse C(biph)−M−H−C angles (165.7°, **3**; 166.7°, **4** vs 150.6°, **1**; 151.7, **2**). The latter are more in line with pincers of type **C**, which feature persistent ε-agostic interactions in solution (Figure 1).[7]

Table 3. Calculated Geometric and NBO Properties of 1−4

	PNP-*t*Bu		PNP-Np	
	M = Rh, **1**	M = Ir, **2**	M = Rh, **3**	M = Ir, **4**
M−H−C (Å)	2.975	2.932	2.790	2.731
$\Delta E^2(\sigma_{CH} \rightarrow ML^*)$ (kcal mol^{-1})	5.17	6.55	21.07	26.20
$\Delta E^2(ML \rightarrow \sigma_{CH}^*)$ (kcal mol^{-1})	3.75	7.69	11.42	18.59
occupancy σ_{CH}	1.961	1.946	1.919	1.893
occupancy σ^*_{CH}	0.009	0.010	0.015	0.022

2.5. Reactivity of 3 and 4 with Carbon Monoxide. Treatment of **3** and **4** with CO (1 atm) in DFB at room temperature resulted in immediate conversion into the corresponding carbonyl derivatives [M(PNP-Np)(biph)(CO)][BAr$^F_4$] (M = Rh, **10**, δ_{31P} 23.2, $^1J_{RhP}$ = 96 Hz; Ir, **11**, δ_{31P} −7.1) in quantitative spectroscopic yield (Scheme 4).

Scheme 4. Preparation of M^{III}(CO) Complexes[a]

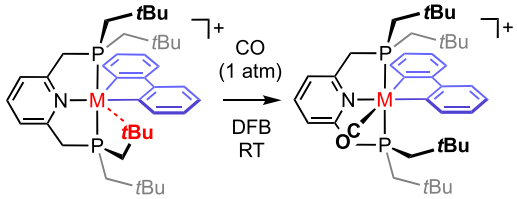

(M = Rh, **3**; Ir, **4**) (M = Rh, **10**; Ir, **11**)

[a] [BAr$^F_4$]$^-$ counterions omitted.

Microcrystalline samples were subsequently obtained from solution by recrystallization from DFB/*n*-hexane in >70% isolated yield, and extensively characterized, including structural elucidation of **11** in the solid state by single-crystal X-ray diffraction (Figure 6). Coordination of CO arrests biph pseudorotation, conferring static C_s symmetry in CD_2Cl_2

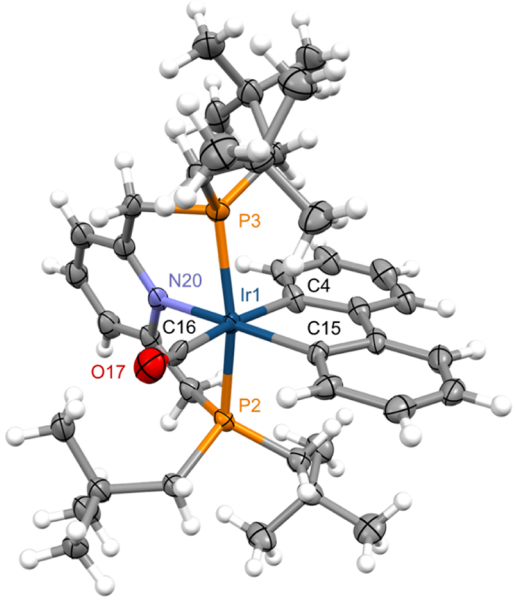

Figure 6. Solid-state structure of iridium(III) carbonyl **11**; ellipsoids drawn at 30% probability and anions omitted for clarity. Selected bond lengths (Å) and angles (deg): Ir1−P2, 2.322(3); Ir1−P3, 2.365(3); Ir1−N20, 2.148(6); Ir1−C4, 2.025(13); Ir1−C15, 2.064(8); Ir1−C16, 1.942(10), C16−O17, 1.145(13); P2−Ir1−P3, 164.20(10); N20−Ir1−C15, 168.9(3); C4−Ir1−C16, 170.8(4).

https://doi.org/10.1021/acs.organomet.4c00081
Organometallics 2024, 43, 1143−1154

solution, and is further evidenced by ^{13}C resonances at δ 189.7 ($^{1}J_{RhC}$ = 44 Hz, $^{2}J_{PC}$ = 10 Hz) and 177.5 ($^{2}J_{PC}$ = 7 Hz) and red-shifted ν(CO) bands at 2056 and 2027 cm^{-1} for **10** and **11** in CH_2Cl_2 solution, respectively. These outcomes contrast the reactivity of **1** and **2** with CO, where under similar conditions no reaction was observed for the former, and slow conversion into a carbonyl derivative occurred for the latter (t = 6 h). Given that we have established that PNP-Np is a considerably weaker net doner than PNP-*t*Bu,[22] this difference in reactivity is best reconciled by the considerably more flexible nature of the Np groups. Indeed, from inspection of the solid-state structures of the homologous series of Ir^{III}(biph) complexes **4**, **9** (Figure 3), and **11** (Figure 6), a broad range of Np conformations is apparent, with the proximal *t*Bu groups being projected away from the chloro and carbonyl ligands in the lattermost examples.

3. SUMMARY

We have described the synthesis and characterization of rhodium(III) and iridium(III) 2,2′-biphenyl complexes that complete a homologous series of five-coordinate PNP pincers **1**–**4**, where the terminal P-donors of the pincer ligand are substituted with either *tert*-butyl or neopentyl groups (Figure 7).

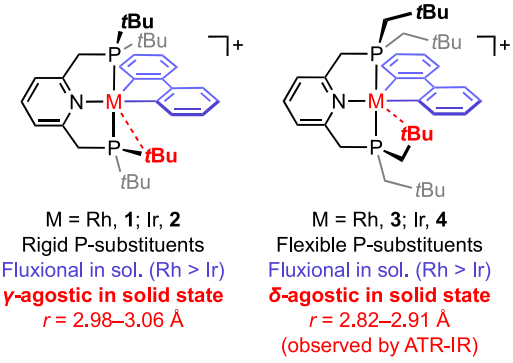

Figure 7. Summary of discussion.

The new neopentyl-substituted examples **3** and **4** were prepared by halide ion abstraction from coordinatively saturated chloro precursors (**8** and **9**) and notable for the adoption of δ-agostic interactions in the solid state by X-ray crystallography and ATR-IR spectroscopy. These agostic interactions do not persist in solution, where pseudorotation of the biphenyl ligand was observed and quantified by variable-temperature ^{1}H NMR spectroscopy. The associated activation barriers are not statistically different to those previously measured for the respective *tert*-butyl-substituted analogues **1** and **2** but are consistent with the adoption of stronger agostic interactions in **3** and **4**, taking into account the relative steric bulk of the P-substituents and supported by the solid-state metrics. The strength of the agostic interactions in **1**–**4** was quantified by DFT-based NBO analysis and, in agreement with the experimental observations, calculated to be greater for M = Ir > Rh (cf. 1.5× greater perturbation energies) and pincer ligand = PNP-Np > PNP-*t*Bu (cf. 3.3× greater perturbation energies). The latter vindicates our hypothesis that more flexible phosphine substituents enable adoption of stronger agostic interactions and is despite the neopentyl-substituted pincer ligand being a weaker net donor than the *tert*-butyl analogue. The fluxional behavior of **3** and **4** is arrested by rapid reaction with CO, conferring coordinatively saturated carbonyl derivatives in both cases and underscores the flexible nature of the P-substituents by reference to the reactivity of **1** (no reaction) and **2** (slow reaction).

4. EXPERIMENTAL SECTION

4.1. General Methods. All manipulations were performed under an atmosphere of argon using Schlenk and glovebox techniques unless otherwise stated. Glassware was oven-dried at 150 °C overnight and flame-dried under vacuum prior to use. Molecular sieves were activated by heating at 300 °C *in vacuo* overnight. PhF and DFB were purchased from Fluorochem, predried over neutral Al_2O_3 for 4 h, dried over CaH_2 overnight before being vacuum-distilled, freeze–pump–thaw degassed, and finally dried over two batches of 3 Å molecular sieves.[14] CD_2Cl_2 was freeze–pump–thaw degassed and dried over 3 Å molecular sieves. C_6D_6 and $SiMe_4$ were dried over Na overnight, distilled, freeze–pump–thaw degassed, and stored over a K mirror. THF was vacuum-distilled from Na/benzophenone and stored over 3 Å molecular sieves. Anhydrous *n*-hexane was purchased from Sigma-Aldrich, sparged with argon, and stored over 3 Å molecular sieves. Et_2NH was dried over CaH_2 overnight before being vacuum-distilled and freeze–pump–thaw degassed prior to use. Other anhydrous solvents were purchased from Acros Organics or Sigma-Aldrich, freeze–pump–thaw degassed, and stored over 3 Å molecular sieves. Np_2PCl,[23] $[Ir(COD)_2][BAr^F{}_4]$,[24] [Rh(dtbpm)(biph)Cl], $[Ir(biph)(COD)Cl]_2$,[16] and $Na[BAr^F{}_4]$[25] were prepared using published procedures. $[Rh(CO)_2Cl]_2$ was prepared by treatment of $[Rh(cyclooctene)_2Cl]_2$[26] with CO (1 atm) and subsequent recrystallization from *n*-hexane. 2,6-Lutidine and TMEDA were dried over Na and benzophenone overnight, vacuum-distilled, freeze–pump–thaw degassed, and stored over 3 Å molecular sieves. $BH_3{\cdot}SMe_2$ was freeze–pump–thaw degassed prior to use. All other reagents are commercial products, and were used as received. NMR spectra were recorded on Bruker spectrometers under an argon atmosphere at 298 K unless otherwise stated. ^{11}B and ^{31}P NMR spectra were referenced externally to $Et_2O{\cdot}BF_3$ and 85% H_3PO_4 standards, respectively. Chemical shifts are quoted in ppm and coupling constants in Hz. Virtual coupling constants are reported as the separation between the first and third lines.[27] In low symmetry complexes, the inequivalent groups distal from the Cl/C–H/CO ligand are labeled (when possible) with a prime. High-resolution (HR) electrospray ionization mass spectrometry (ESI-MS) was recorded on a Bruker Maxis Plus instrument. Microanalyses were performed at Elemental Microanalysis Ltd.

4.2. Preparation of PNP-Np. Step 1. A solution of 2,6-lutidine (0.20 mL, 1.7 mmol) and TMEDA (0.55 mL, 3.7 mmol) in Et_2O (10 mL) was cooled to 0 °C, and ^{n}BuLi (1.6 M in hexanes, 2.5 mL, 4.0 mmol) was added dropwise. The colorless solution turned orange immediately and was stirred at room temperature for a further 21 h. The solution was then cooled to −78 °C, and a solution of Np_2PCl (3.78 mmol) in Et_2O (10 mL) was added dropwise. The solution turned yellow with the precipitation of a white solid, and the mixture was heated at 30 °C for 92 h. The yellow solution was filtered, and volatiles were removed under reduced pressure to afford 0.88 g of crude PNP-Np, which was used without further purification.

Step 2. A solution of crude PNP-Np (0.88 g) in THF (15 mL) was cooled to −78 °C, and $BH_3{\cdot}SMe_2$ (0.41 mL, 4.3 mmol) was added. The resulting mixture was stirred at room temperature for 30 min before quenching with saturated aqueous NH_4Cl (20 mL). The organic phase was extracted, dried over $MgSO_4$, and filtered. Volatiles were removed under reduced pressure to afford a white solid, which was purified via column chromatography (7:3 v/v CH_2Cl_2/*n*-hexane, R_F = 0.45). Yield: 0.53 g (1.1 mmol, 65% with respect to 2,6-lutidine).

Step 3. PNP-Np·$(BH_3)_2$ (0.140 g, 0.292 mmol) was suspended in Et_2NH (20 mL) and heated at reflux for 48 h. Volatiles were removed under reduced pressure to give a white solid. Pentane was added (2 mL) and removed under reduced pressure to form an azeotrope with any remaining Et_2NH. The product was extracted into a small quantity of THF to afford the product as a white solid upon removal of volatiles under reduced pressure. Yield 0.110 g (0.244 mmol, 84%). Data are consistent with the literature.[11]

Data for PNP-Np·$(BH_3)_2$:

https://doi.org/10.1021/acs.organomet.4c00081
Organometallics 2024, 43, 1143−1154

^{1}H NMR ($CDCl_3$, 500 MHz): δ 7.59 (t, $^3J_{HH}$ = 7.7, 1H, 4-py), 7.12 (d, $^3J_{HH}$ = 7.6, 2H, 3-py), 3.19 (d, $^2J_{PH}$ = 9.9, 4H, pyC$\underline{H}_2$), 1.87 (dd, $^2J_{PH}$ = 14.9, $^2J_{HH}$ = 12.2, 4H, C$\underline{H}_2$*t*Bu), 1.56 (dd, $^2J_{HH}$ = 10.5, $^2J_{PH}$ = 4.3, 4H, C$\underline{H}_2$*t*Bu), 1.13 (s, 36H, *t*Bu), 0.4−1.4 (obscured partially collapsed quartet, 6H, BH_3).

^{13}C{^{1}H} NMR ($CDCl_3$, 126 MHz): δ 154.3 (dd, $^2J_{PC}$ = 8, $^4J_{PC}$ = 2, 2-py), 136.8 (s, 4-py), 123.4 (dd, $^3J_{PC}$ = 4, $^5J_{PC}$ = 2, 3-py), 39.4 (d, $^1J_{PC}$ = 28, $\underline{C}H_2$*t*Bu), 38.6 (d, $^1J_{PC}$ = 30, py$\underline{C}H_2$), 32.4 (s, *t*Bu{C}), 31.6 (d, $^3J_{PC}$ = 6, *t*Bu{CH_3}).

^{31}P{^{1}H} NMR ($CDCl_3$, 162 MHz): δ 10.7 (partially collapsed quartet, fwhm = 125 Hz).

^{11}B{^{1}H} NMR ($CDCl_3$, 96 MHz): δ −35.9 (br).

HR ESI-MS (positive ion, 4 kV): 502.4050 ($[M+Na]^+$, calcd 502.4054) *m*/*z*.

Data for PNP-Np:

^{1}H NMR (C_6D_6, 500 MHz): δ 7.07 (t, $^3J_{HH}$ = 7.7, 1H, 4-py), 6.79 (d, $^3J_{HH}$ = 7.6, 2H, 3-py), 2.96 (d, $^2J_{PH}$ = 1.8, 4H, pyC$\underline{H}_2$), 1.77 (dd, $^2J_{HH}$ = 14.2, $^2J_{PH}$ = 4.1, 4H, C$\underline{H}_2$*t*Bu), 1.29 (dd, $^2J_{HH}$ = 14.2, $^2J_{PH}$ = 3.3, 4H, C$\underline{H}_2$*t*Bu), 1.05 (s, 36H, *t*Bu).

^{13}C{^{1}H} NMR (C_6D_6, 126 MHz): δ 159.1 (d, $^2J_{PC}$ = 4, 2-py), 135.8 (s, 4-py), 120.6 (dd, $^3J_{PC}$ = 5, $^5J_{PC}$ = 2, 3-py), 44.8 (d, $^1J_{PC}$ = 18, $\underline{C}H_2$*t*Bu), 40.4 (d, $^1J_{PC}$ = 18, py$\underline{C}H_2$), 31.7 (d, $^2J_{PC}$ = 15, *t*Bu{C}), 31.1 (d, $^3J_{PC}$ = 9, *t*Bu{CH_3}).

^{31}P{^{1}H} NMR (C_6D_6, 162 MHz): δ −39.9 (s).

HR ESI-MS (positive ion, 4 kV): 452.3559 ($[M+H]^+$, calcd 452.3570) *m*/*z*.

4.3. Preparation of [Rh(PNP-Np)(CO)][BAr$^F_4$] 5. A solution of PNP-Np (12.1 mg, 26.8 μmol) in PhF (0.5 mL) was transferred into a J Young valve NMR tube charged with $[Rh(CO)_2Cl]_2$ (5.3 mg, 14 μmol) and Na[BAr$^F_4$] (27.0 mg, 30.5 μmol) and agitated at room temperature for 30 min. The yellow solution was filtered, and volatiles were removed under reduced pressure to give a yellow residue, which was washed with *n*-hexane (0.5 mL) and dried. The resulting solid was extracted into CH_2Cl_2, and volatiles were removed under reduced pressure to afford the product as a yellow solid. Yield: 28.4 mg (19.6 μmol, 73%). Single crystals suitable for X-ray diffraction were obtained by slow diffusion of *n*-hexane into a CD_2Cl_2 solution at ambient temperature.

^{1}H NMR (CD_2Cl_2, 500 MHz): δ 7.76 (t, $^3J_{HH}$ = 7.8, 1H, 4-py), 7.71−7.74 (m, 8H, Ar^F), 7.56 (br, 4H, Ar^F), 7.38 (d, $^3J_{HH}$ = 7.8, 2H, 3-py), 3.85 (vt, J_{PC} = 8.5, 4H, pyC$\underline{H}_2$), 2.09 (dvt, $^2J_{HH}$ = 14.8, J_{PH} = 5.7, 4H, C$\underline{H}_2$*t*Bu), 2.01 (dm, $^2J_{HH}$ = 14.8, 4H, C$\underline{H}_2$*t*Bu), 1.17 (s, 36H, *t*Bu).

^{13}C{^{1}H} NMR (CD_2Cl_2, 126 MHz): δ 193.4 (dt, $^1J_{RhC}$ = 71, $^2J_{PC}$ = 15, CO), 163 (obscured, 2-py), 162.2 (q, $^1J_{CB}$ = 50, Ar^F), 141.0 (s, 4-py), 135.2 (s, Ar^F), 129.3 (qq, $^2J_{FC}$ = 32, $^3J_{CB}$ = 3, Ar^F), 125.0 (q, $^1J_{FC}$ = 272, CF_3), 122.7 (vt, J_{PC} = 11, 3-py), 117.9 (sept, $^3J_{FC}$ = 4, Ar^F), 46.2 (vtd, J_{PC} = 25, $^2J_{RhC}$ = 1, $\underline{C}H_2$*t*Bu), 45.5 (vt, J_{PC} = 23, py$\underline{C}H_2$), 32.0 (s, *t*Bu{C}), 31.9 (vt, J_{PC} = 6, *t*Bu{CH_3}).

^{31}P{^{1}H} NMR (CD_2Cl_2, 162 MHz): δ 17.4 (d, $^1J_{RhP}$ = 121).

IR (CH_2Cl_2): ν(CO) = 2004 cm^{-1}. **ATR-IR**: ν(CO) = 2010 cm^{-1}.

HR ESI-MS (positive ion, 4 kV): 582.2489 ($[M]^+$, calcd 582.2495) *m*/*z*.

Anal. Calcd for $C_{60}H_{63}BF_{24}NOP_2Rh$ (1445.79 g mol^{-1}): C, 49.85; H, 4.39; N, 0.97; found: C, 50.08; H, 4.32; N, 0.98.

4.4. Preparation of of [Ir(PNP-Np)(CO)][BAr$^F_4$] 6. Step 1, Preparation of [Ir(PNP-Np′)H][BAr$^F_4$] 7. In a modification of the procedure reported by Yamashita and Nozaki,[11] PNP-Np (20.1 mg, 44.5 μmol) and $[Ir(COD)_2][BAr^F_4]$ (57.0 mg, 44.8 μmol) were dissolved in DFB (10 mL), and the red solution was stirred at room temperature for 30 min. Volatiles were removed under reduced pressure to give the product as a deep red solid, which was washed with *n*-hexane (5 mL) and dried. Yield: 43.9 mg (29.1 μmol, 65%). Data are consistent with the literature.[11] Single crystals suitable for X-ray diffraction were obtained by slow diffusion of *n*-hexane into a DFB solution at room temperature.

Step 2. In a modification of the procedure reported by Yamashita and Nozaki, a solution of [Ir(PNP-Np′)H][BAr$^F_4$] (8.0 mg, 5.3 μmol) in DFB (0.5 mL) was prepared in a J Young valve NMR tube, freeze−pump−thaw degassed, placed under CO (1 atm), and then gently shaken at room temperature. An immediate color change from red to pale yellow was observed. Volatiles were removed under reduced pressure, and the resulting residue was washed with *n*-hexane (0.5 mL) and dried *in vacuo*. This procedure afforded 7.2 mg of the crude product as a yellow solid in ∼91% purity (by ^{31}P{^{1}H} NMR), which was used for IR analysis without further purification. Data are consistent with the literature.[11]

Data for [Ir(PNP-Np′)H][BAr$^F_4$] **7**:

^{1}H NMR (CD_2Cl_2, 500 MHz): δ 7.80 (t, $^3J_{HH}$ = 7.8, 1H, 4-py), 7.70−7.74 (m, 8H, Ar^F), 7.56 (s, 4H, Ar^F), 7.51 (d, $^3J_{HH}$ = 7.7, 2H, 3,5-py), 4.05−4.16 (m, 1H, pyC$\underline{H}_2$), 3.80−3.95 (m, 2H, 2× pyC$\underline{H}_2$), 3.55 (dd, $^2J_{HH}$ = 17.1, $^2J_{PH}$ = 8.4, 1H, pyC$\underline{H}_2$), 2.67 (br m, 1H, IrCH_2), 2.49 (dd, $^2J_{HH}$ = 15.2, $^2J_{PH}$ = 8.0, 1H, C$\underline{H}_2$*t*Bu), 2.42 (dd, $^2J_{HH}$ = 15.8, $^2J_{PH}$ = 9.6, 1H, C$\underline{H}_2$*t*Bu), 2.14−2.28 (m, 2H, 2× C$\underline{H}_2$*t*Bu), 2.06 (dd, $^2J_{HH}$ = 14.8, $^2J_{PH}$ = 6.2, 1H, C$\underline{H}_2$*t*Bu), 1.74 (dd, $^2J_{HH}$ = 14.6, $^2J_{PH}$ = 10.4, 1H, C$\underline{H}_2$*t*Bu), 1.55−1.64 (m, 1H, PC$\underline{H}_2$CMe_2CH_2Ir), 1.23 (s, 9H, *t*Bu{PNp_2}), 1.18 (s, 9H, *t*Bu{PNp′}), 1.05 (s, 3H, $PCH_2C\underline{Me}_2CH_2$Ir), 1.01 (s, 3H, $PCH_2C\underline{Me}_2CH_2$Ir), 0.81−0.92 (m, 2H, PC$\underline{H}_2$CMe_2C$\underline{H}_2$Ir), 0.38 (s, 9H, *t*Bu{PNp_2}), −16.81 (t, $^2J_{PH}$ = 12, 1H, IrH).

^{31}P{^{1}H} NMR (CD_2Cl_2, 162 MHz): δ 28.5 (d, $^2J_{PP}$ = 316, 1P, PNp′), 18.5 (d, $^2J_{PP}$ = 316, PNp_2).

HR ESI-MS (positive ion, 4 kV): 644.3115 ($[M]^+$, calcd 644.3122) *m*/*z*.

Data for [Ir(PNP-Np)(CO)][BAr$^F_4$] **6**:

^{1}H NMR (CD_2Cl_2, 500 MHz): δ 7.87 (t, $^3J_{HH}$ = 7.8, 1H, 4-py, 1H), 7.69−7.74 (m, 8H, Ar^F), 7.56 (br, 4H, Ar^F), 7.49 (d, $^3J_{HH}$ = 7.8, 2H, 3-py), 3.93 (vt, J_{PH} = 8.7, 4H, pyC$\underline{H}_2$), 2.23 (dvt, $^2J_{HH}$ = 14.9, J_{PH} = 8.1, 4H, C$\underline{H}_2$*t*Bu), 2.16 (dvt, $^2J_{HH}$ = 14.9, J_{PH} = 6.3, 4H, C$\underline{H}_2$*t*Bu), 1.17 (s, 36H, *t*Bu).

^{31}P{^{1}H} NMR (CD_2Cl_2, 162 MHz): δ 13.6 (s).

IR (CH_2Cl_2): ν(CO) = 1991 cm^{-1}. **ATR-IR**: ν(CO) = 1999 cm^{-1}.

HR ESI-MS (positive ion, 4 kV): 672.3070 ($[M]^+$, calcd 672.3071) *m*/*z*.

4.5. Preparation of [Rh(PNP-Np)(biph)Cl] 8. A suspension of PNP-Np (111.0 mg, 0.246 mmol) and [Rh(biph)(dtbpm)Cl] (146.3 mg, 0.246 mmol) in PhF (10 mL) was heated at reflux for 18 h. Volatiles were removed under reduced pressure to give an orange residue, which was extracted into CH_2Cl_2 (10 mL), and the product was isolated as an off-white solid upon removal of volatiles, which was washed with pentane (3 × 5 mL) and dried. Yield: 128.6 mg (0.173 mmol, 70%). Single crystals suitable for X-ray diffraction were obtained by slow diffusion of $SiMe_4$ into a CH_2Cl_2 solution at −30 °C.

^{1}H NMR (CD_2Cl_2, 600 MHz): δ 8.04 (d, $^3J_{HH}$ = 7.5, 1H, 6-biph), 7.72 (t, $^3J_{HH}$ = 7.8, 1H, 4-py), 7.49 (dd, $^3J_{HH}$ = 7.6, $^4J_{HH}$ = 1.5, 1H, 3′-biph), 7.42 (dd, $^3J_{HH}$ = 7.5, $^4J_{HH}$ = 1.5, 1H, 3-biph), 7.37 (d, $^3J_{HH}$ = 7.8, 2H, 3-py), 6.92 (t, $^3J_{HH}$ = 7.3, 1H, 4′-biph), 6.88 (t, $^3J_{HH}$ = 7.3, 1H, 4-biph), 6.82 (td, $^3J_{HH}$ = 7.3, $^4J_{HH}$ = 1.5, 1H, 5-biph), 6.64 (td, $^3J_{HH}$ = 7.4, $^4J_{HH}$ = 1.5, 1H, 5′-biph), 6.29 (d, $^3J_{HH}$ = 7.5, 1H, 6′-biph), 4.14 (dvt, $^2J_{HH}$ = 16.1, J_{PH} = 9.0, 2H, pyC$\underline{H}_2$), 3.96 (dvt, $^2J_{HH}$ = 16.1, J_{PH} = 8.2, 2H, pyC$\underline{H}_2$′), 2.38 (dvtd, $^2J_{HH}$ = 14.7, J_{PH} = 7.2, $^3J_{RhH}$ = 1.3, 2H, C$\underline{H}_2$*t*Bu), 2.28 (dvt, $^2J_{HH}$ = 14.7, J_{PH} = 6.0, 2H, C$\underline{H}_2$*t*Bu), 1.42 (d app q, $^2J_{HH}$ = 15.4, J = 1.9, 2H, C$\underline{H}_2$*t*Bu′), 1.30 (dvt, $^2J_{HH}$ = 15.4, J_{PH} = 5.8, 2H, C$\underline{H}_2$*t*Bu′), 1.01 (s, 18H, *t*Bu), 0.58 (s, 18H, *t*Bu′).

^{13}C{^{1}H} NMR (CD_2Cl_2, 126 MHz): δ 166.4 (dt, $^1J_{RhC}$ = 35, $^2J_{PC}$ = 9, 1′-biph), 165.7 (dt, $^1J_{RhC}$ = 30, $^2J_{PC}$ = 9, 1-biph), 160.3 (vt, J_{PC} = 7, 2-py), 155.1 (br, 2′-biph), 151.9 (br, 2-biph), 137.9 (s, 6-biph), 137.4 (s, 4-py), 133.7 (t, $^2J_{PC}$ = 2, 6′-biph), 125.2 (s, 5′-biph), 124.5 (s, 5-biph), 122.6 (s, 4′-biph), 121.6 (vt, J_{PC} = 10, 3-py), 121.3 (s, 4-biph), 120.7 (s, 3′-biph), 119.3 (s, 3-biph), 43.3 (vt, J_{PC} = 22, py$\underline{C}H_2$), 37.9 (vt, J_{PC} = 18, $\underline{C}H_2$*t*Bu), 33.6 (vtd, J_{PC} = 16, $^2J_{RhC}$ = 3, $\underline{C}H_2$*t*Bu′), 32.5 (vt, J_{PC} = 6, *t*Bu{CH_3}), 32.2 (vt, J_{PC} = 6, *t*Bu{C}), 32.04 (br, *t*Bu′{C}), 31.95 (vt, J_{PC} = 5, *t*Bu′{CH_3}).

^{31}P{^{1}H} NMR (CD_2Cl_2, 243 MHz): δ 26.2 (d, $^1J_{RhP}$ = 109).

HR ESI-MS (positive ion, 4 kV): 706.3166 ($[M-Cl]^+$, calcd 706.3172) *m*/*z*.

Anal. Calcd for $C_{39}H_{59}ClNP_2Rh$ (742.21 g mol^{-1}): C, 63.11; H, 8.01; N, 1.89; Found: C, 63.39; H, 7.88; N, 1.79.

4.6. Preparation of [Ir(PNP-Np)(biph)Cl] 9. A suspension of PNP-Np (108.3 mg, 0.240 mmol) and $[Ir(biph)(COD)Cl]_2$ (93.7 mg, 0.0960 mmol) in PhF (10 mL) was heated at reflux for 24 h, giving a yellow solution. Volatiles were removed under reduced pressure to

https://doi.org/10.1021/acs.organomet.4c00081
Organometallics 2024, 43, 1143−1154

afford the product as a pale yellow solid, which was washed with pentane (3 × 5 mL) and dried. Yield: 127 mg (0.153 mmol, 64%). Single crystals suitable for X-ray diffraction were obtained by slow diffusion of *n*-hexane into a PhF solution at −30 °C.

^{1}H NMR (CD_2Cl_2, 600 MHz): δ 7.91 (d, $^3J_{HH}$ = 7.4, 1H, 6-biph), 7.76 (t, $^3J_{HH}$ = 7.8, 1H, 4-py), 7.46 (dd, $^3J_{HH}$ = 7.6, $^4J_{HH}$ = 1.5, 1H, 3′-biph), 7.41 (d, $^3J_{HH}$ = 7.8, 2H, 3-py), 7.40 (dd, $^3J_{HH}$ = 7.5, $^4J_{HH}$ = 1.4, 1H, 3-biph), 6.88 (t, $^3J_{HH}$ = 7.3, 1H, 4′-biph), 6.84 (t, $^3J_{HH}$ = 7.2, 1H, 4-biph), 6.78 (td, $^3J_{HH}$ = 7.3, $^4J_{HH}$ = 1.5, 1H, 5-biph), 6.57 (td, $^3J_{HH}$ = 7.3, $^4J_{HH}$ = 1.5, 1H, 5′-biph), 6.26 (d, $^3J_{HH}$ = 7.4, 1H, 6′-biph), 4.09 (dvt, $^2J_{HH}$ = 16.2, J_{PH} = 9.3, 2H, pyC$\underline{H}_2$), 3.99 (dvt, $^2J_{HH}$ = 16.2, J_{PH} = 8.6, 2H, pyC$\underline{H}_2$′), 2.39 (dvt, $^2J_{HH}$ = 14.7, J_{PH} = 7.2, 2H, C$\underline{H}_2$*t*Bu), 2.25 (dvt, $^2J_{HH}$ = 14.7, J_{PH} = 7.0, 2H, C$\underline{H}_2$*t*Bu), 1.50 (dvt, $^2J_{HH}$ = 15.4, J_{PH} = 4.6, 2H, C$\underline{H}_2$*t*Bu′), 1.32 (dvt, $^2J_{HH}$ = 15.3, J_{PH} = 6.8, 2H, C$\underline{H}_2$*t*Bu′), 1.01 (s, 18H, *t*Bu), 0.58 (s, 18H, *t*Bu′).

^{13}C{^{1}H} NMR (CD_2Cl_2, 126 MHz): δ 161.7 (vt, J_{PC} = 6, 2-py), 156.1 (s, 2′-biph), 153.2 (s, 2-biph), 145.6 (t, $^2J_{PC}$ = 7, 1-biph), 145.0 (t, $^2J_{PC}$ = 7, 1′-biph), 137.6 (s, 4-py), 136.6 (s, 6-biph), 132.0 (s, 6′-biph), 125.3 (s, 5′-biph), 124.8 (s, 5-biph), 122.0 (s, 4′-biph), 121.3 (vt, J_{PC} = 9, 3-py), 120.7 (s, 3′-biph), 120.6 (s, 4-biph), 119.3 (s, 3-biph), 43.6 (vt, J_{PC} = 27, py$\underline{C}H_2$), 36.8 (vt, J_{PC} = 23, $\underline{C}H_2$*t*Bu), 32.4 (vt, J_{PC} = 6, *t*Bu{CH_3}), 32.3 (vt, J_{PC} = 22, $\underline{C}H_2$*t*Bu′), 32.0 (vt, J_{PC} = 6, *t*Bu/*t*Bu′{C}), 31.9 (vt, J_{PC} = 5, *t*Bu/*t*Bu′{C}), 32.3 (vt, J_{PC} = 6, *t*Bu′{CH_3}).

^{31}P{^{1}H} NMR (CD_2Cl_2, 243 MHz): δ 0.6 (s).

HR ESI-MS (positive ion, 4 kV): 796.3743 ([M−Cl]$^+$, calcd 796.3749) *m*/*z*.

Anal. Calcd for $C_{39}H_{59}ClNIrP_2$ (831.52 g mol^{-1}): C, 56.33; H, 7.15; N, 1.68; found: C, 56.02; H, 7.12; N, 1.64.

4.7. Preparation of [Rh(PNP-Np)(biph)][BAr$^F_4$] 3. A suspension of [Rh(PNP-Np)(biph)Cl] (94.4 mg, 0.127 mmol) and Na[BAr$^F_4$] (113.5 mg, 0.128 mmol) in PhF (10 mL) was stirred at room temperature for 30 min. The solution was filtered, and the product was obtained as a yellow solid upon removal of volatiles, which was washed with pentane (5 mL) and dried. Yield: 172 mg (0.109 mmol, 86%). Single crystals suitable for X-ray diffraction were obtained by slow diffusion of $SiMe_4$ into a CH_2Cl_2/*n*-hexane solution at −30 °C.

^{1}H NMR (CD_2Cl_2, 200 K, 500 MHz): δ 7.84 (t, $^3J_{HH}$ = 7.8, 1H, 4-py), 7.70−7.75 (m, 8H, Ar^F), 7.53 (obs d, $^3J_{HH}$ = 8, 2H, 3-py), 7.53 (br, 4H, Ar^F), 7.51 (obs d, $^3J_{HH}$ = 7, 1H, 3-biph), 7.46 (app d, 2H, $^3J_{HH}$ = 8, 6-biph + 3′-biph), 7.04 (t, $^3J_{HH}$ = 7.4, 1H, 4-biph), 6.98 (obs t, $^3J_{HH}$ = 7, 1H, 4′-biph), 6.96 (obs t, $^3J_{HH}$ = 7, 1H, 5-biph), 6.63 (t, $^3J_{HH}$ = 7.5, 1H, 5′-biph), 5.71 (d, $^3J_{HH}$ = 7.9, 1H, 6′-biph), 3.88 (vt, J_{PH} = 8.0, 4H, pyC$\underline{H}_2$ + pyC$\underline{H}_2$′), 2.23 (d, $^2J_{HH}$ = 15.2, 2H, C$\underline{H}_2$*t*Bu), 1.79 (dvt, $^2J_{HH}$ = 15.2, J_{PH} = 7.0, 2H, C$\underline{H}_2$*t*Bu), 1.36 (dvt, $^2J_{HH}$ = 15.2, J_{PH} = 7.4, 2H, C$\underline{H}_2$*t*Bu′), 1.26 (dvt, $^2J_{HH}$ = 15.2, J_{PH} = 5.4, 2H, C$\underline{H}_2$*t*Bu′), 0.83 (s, 18H, *t*Bu), 0.49 (s, 18H, *t*Bu′).

^{31}P{^{1}H} NMR (CD_2Cl_2, 202 MHz): δ 23.8 (d, $^1J_{RhP}$ = 111).

^{31}P{^{1}H} NMR (CD_2Cl_2, 200 K, 202 MHz): δ 26.9 (d, $^1J_{RhP}$ = 109).

ATR-IR: ν(agostic CH) = 2682 cm^{-1}.

HR ESI-MS (positive ion, 4 kV): 706.3166 ([M]$^+$, calcd 706.3172) *m*/*z*.

Anal. Calcd for $C_{71}H_{71}BF_{24}NP_2Rh$ (1569.98 g mol^{-1}): C, 54.32; H, 4.56; N, 0.89; found: C, 54.67; H, 4.49; N, 0.92.

4.8. Preparation of [Ir(PNP-Np)(biph)][BAr$^F_4$] 4. A suspension of [Ir(PNP-Np)(biph)Cl] (106.4 mg, 0.128 mmol) and Na[BAr$^F_4$] (124.1 mg, 0.140 mmol) in PhF (10 mL) was stirred at room temperature for 1 h. The solution was filtered, and the product was obtained as an orange solid upon removal of volatiles, washed with pentane (5 mL), and dried. Yield: 177.3 mg (1.07 mmol, 84%). Single crystals suitable for X-ray diffraction were obtained by slow diffusion of $SiMe_4$ into a CH_2Cl_2 solution at −30 °C.

^{1}H NMR (CD_2Cl_2, 200 K, 500 MHz): δ 7.88 (t, $^3J_{HH}$ = 7.8, 1H, 4-py), 7.71−7.75 (m, 8H, Ar^F), 7.60 (d, $^3J_{HH}$ = 7.8, 2H, 3-py), 7.53 (br, 4H, Ar^F), 7.51 (d, $^3J_{HH}$ = 7.7, 1H, 3-biph), 7.47 (d, $^3J_{HH}$ = 7.4, 1H, 6-biph), 7.42 (d, $^3J_{HH}$ = 7.6, 1H, 3′-biph), 6.99 (t, $^3J_{HH}$ = 7.4, 1H, 4-biph), 6.93 (t, $^3J_{HH}$ = 7.4, 1H, 5-biph), 6.92 (t, $^3J_{HH}$ = 7.4, 1H, 4′-biph), 6.53 (t, $^3J_{HH}$ = 7.5, 1H, 5′-biph), 5.60 (d, $^3J_{HH}$ = 7.8, 1H, 6′-biph), 3.96 (dvt, $^2J_{HH}$ = 17.0, J_{PH} = 8.8, 2H, pyC$\underline{H}_2$′), 3.87 (dvt, $^2J_{HH}$ = 17.0, J_{PH} = 8.1, 2H, pyC$\underline{H}_2$), 2.36 (d, $^2J_{HH}$ = 15.4, 2H, C$\underline{H}_2$*t*Bu), 1.75 (dvt, $^2J_{HH}$ = 15.4, J_{PH} = 8.2, 2H, C$\underline{H}_2$*t*Bu), 1.42 (dvt, $^2J_{HH}$ = 15.5, J_{PH} = 7.6, 2H, C$\underline{H}_2$*t*Bu′), 1.30 (dvt, $^2J_{HH}$ = 15.5, J_{PH} = 6.2, 2H, C$\underline{H}_2$*t*Bu′), 0.79 (s, 18H, *t*Bu), 0.48 (s, 18H, *t*Bu′).

^{31}P{^{1}H} NMR (CD_2Cl_2, 202 MHz): δ 11.2 (s).

^{31}P{^{1}H} NMR (CD_2Cl_2, 200 K, 202 MHz): δ 12.6 (s).

ATR-IR: ν(agostic CH) = 2579 cm^{-1}.

HR ESI-MS (positive ion, 4 kV): 796.3755 ([M]$^+$, calcd 796.3749) *m*/*z*.

Anal. Calcd for $C_{71}H_{71}BF_{24}IrNP_2$ (1659.29 g mol^{-1}): C, 51.39; H, 4.31; N, 0.84; found: C, 51.52; H, 4.19; N, 0.87.

4.9. Analysis of 3 and 4 by Variable-Temperature NMR Spectroscopy. Data were collected using 20 mM solutions of **3** and **4** in CD_2Cl_2 (0.6 mL) within a flame-sealed NMR tube on a 500 MHz Bruker spectrometer. Samples were equilibrated at the required temperature for at least 5 min before data were acquired. The line fitting modeled the exchange rates on the C$\underline{H}_2$*t*Bu signals using the gNMR software version 4.1.2.[19] Reference line widths and coupling constants were fixed following analysis of low-temperature data. Activation parameters were determined by Eyring analysis of the associated rate constants (see SI).

Table 4. Rate Constants and Thermodynamic Data for 3:

T (K)	log(k_{exch})	k_{exch} (s^{-1})	ln(k_{exch}/T)
225	−0.4507	0.35	−6.454
250	0.8156	6.54	−3.643
273	1.8307	67.72	−1.394
298	2.7600	575.44	0.658
308	3.0590	1145.51	1.314

$\Delta H^{\ddagger}$ = 54.2 ± 0.4 kJ mol^{-1}
$\Delta S^{\ddagger}$ = −10.4 ± 1.5 J mol^{-1} K^{-1}
$\Delta G_{298\ K}^{\ddagger}$ = 57.3 ± 0.8 kJ mol^{-1}

Table 5. Rate Constants and Thermodynamic Data for 4:

T (K)	log(k_{exch})	k_{exch} (s^{-1})	ln(k_{exch}/T)
283	0.6922	4.92	−4.052
288	1.0109	10.25	−3.335
293	1.2807	19.09	−2.731
298	1.5515	35.60	−2.125
303	1.8288	67.42	−1.503
308	2.0796	120.12	−0.942

$\Delta H^{\ddagger}$ = 89.7 ± 0.8 kJ mol^{-1}
$\Delta S^{\ddagger}$ =86.0 ± 2.6 J mol^{-1} K^{-1}
$\Delta G_{298\ K}^{\ddagger}$ = 64.1 ± 1.5 kJ mol^{-1}

4.10. Preparation of [Rh(PNP-Np)(biph)(CO)][BAr$^F_4$] 10. A 20 mM solution of [Rh(PNP-Np)(biph)][BAr$^F_4$] (15.7 mg, 10.0 μmol) in DFB (0.5 mL) was prepared in a J Young valve NMR tube, freeze−pump−thaw degassed, placed under CO (1 atm), and then gently shaken at room temperature. An immediate color change from yellow to colorless was observed. The solution was freeze−pump−thaw degassed and placed under Ar, and the product was obtained as colorless crystals by recrystallization from DFB/*n*-hexane. Yield: 11.4 mg (7.13 μmol, 71%). Satisfactory microanalysis was unable to be obtained for this material, presumably due to partial loss of CO in the solid state over time, which was accelerated by exposure to a dynamic vacuum and was confirmed by dissolution in solution and analysis by NMR spectroscopy.

^{1}H NMR (CD_2Cl_2, 500 MHz): δ 7.95 (t, $^3J_{HH}$ = 7.8, 1H, 4-py), 7.69−7.74 (m, 9H, Ar^F + 3′-biph), 7.64 (dd, $^3J_{HH}$ = 7.7, $^4J_{HH}$ = 1.6, 1H, 3-biph), 7.60 (d, $^3J_{HH}$ = 7.8, 2H, 3-py), 7.54 (m, 5H, 6-biph + Ar^F), 7.17 (t, $^3J_{HH}$ = 7.4, 1H, 4′-biph), 7.12 (t, $^3J_{HH}$ = 7.4, 1H, 4-biph), 6.99 (td, $^3J_{HH}$ = 7.4, $^4J_{HH}$ = 1.5, 1H, 5-biph), 6.87 (t, $^3J_{HH}$ = 7.4, 1H, 5′-biph), 5.96

https://doi.org/10.1021/acs.organomet.4c00081
Organometallics 2024, 43, 1143−1154

(d, $^3J_{HH}$ = 7.6, 1H, 6′-biph), 4.38 (dvt, $^2J_{HH}$ = 17.3, J_{PH} = 9.4, 2H, pyC$\underline{H}_2$′), 3.80 (dvt, $^2J_{HH}$ = 17.3, J_{PH} = 7.4, 2H, pyC$\underline{H}_2$), 2.54 (d app q, $^2J_{HH}$ = 15.2, J = 2.4, 2H, C$\underline{H}_2t$Bu), 2.17 (dvt, $^2J_{HH}$ = 15.2, J_{PH} = 5.2, 2H, C$\underline{H}_2t$Bu),1.29 (dvt, $^2J_{HH}$ = 15.9, J_{PH} = 5.6, 2H, C$\underline{H}_2t$Bu′), 1.19 (dvt, $^2J_{HH}$ = 15.9, J_{PH} = 6.4, 2H, C$\underline{H}_2t$Bu′), 1.00 (s, 18H, tBu), 0.70 (s, 18H, tBu′).

^{13}C{^{1}H} NMR (CD_2Cl_2, 126 MHz): δ 189.7 (dt, $^1J_{RhC}$ = 44, $^2J_{PC}$ = 10, CO), 166.0 (dt, $^1J_{RhC}$ = 26, $^2J_{PC}$ = 9, 1′-biph), 162.2 (q, $^1J_{CB}$ = 50, Ar^F), 159.3 (vt, J_{PC} = 5, 2-py), 155.0 (dt, $^1J_{RhC}$ = 29, $^2J_{PC}$ = 7, 1-biph), 153.1 (s, 2′-biph), 151.3 (s, 2-biph), 140.8 (s, 4-py), 139.0 (s, 6-biph), 135.2 (br, Ar^F), 132.3 (vt, J_{PC} = 4, 6′-biph), 129.3 (qq, $^2J_{FC}$ = 32, $^3J_{CB}$ = 3, Ar^F), 127.8 (s, 5-biph), 127.8 (s, 5′-biph), 126.2 (s, 4′-biph), 125.0 (q, $^1J_{FC}$ = 272, CF_3), 124.7 (s, 4-biph), 123.8 (vt, J_{PC} = 10, 3-py), 123.1 (s, 3′-biph), 122.7 (s, 3-biph), 117.9 (sept, $^3J_{FC}$ = 4, Ar^F), 44.9 (vt, J_{PC} = 21, CH_2tBu), 44.2 (vt, J_{PC} = 24, py$\underline{C}H_2$), 33.9 (vtd, J_{PC} = 19, $^2J_{RhC}$ = 2, CH_2tBu′), 33.3 (vt, J_{PC} = 8, tBu′{C}), 32.7 (s, tBu{C}), 32.3 (vt, J_{PC} = 6, tBu{CH_3}), 31.9 (vt, J_{PC} = 6, tBu′{CH_3}).

^{31}P{^{1}H} NMR (CD_2Cl_2, 162 MHz): δ 23.2 (d, $^1J_{RhP}$ = 96).

IR (CH_2Cl_2): ν(CO) = 2056 cm^{-1}. **ATR-IR**: ν(CO) = 2058 cm^{-1}.

HR ESI-MS (positive ion, 4 kV): 706.3163 ([M−CO]$^+$, calcd 706.3172) m/z.

4.11. Preparation of [Ir(PNP-Np)(biph)(CO)][BAr$^F_4$] 11. A 20 mM solution of [Ir(PNP-Np)(biph)][BAr$^F_4$] (16.6 mg, 10.0 μmol) in DFB (0.5 mL) was prepared in a J Young valve NMR tube, freeze−pump−thaw degassed, placed under CO (1 atm), and then gently shaken at room temperature. An immediate color change from yellow to colorless was observed. The solution was freeze−pump−thaw degassed and placed under Ar, and the product was obtained as colorless crystals by recrystallization from DFB/n-hexane, some of which were suitable for analysis by X-ray diffraction. Yield: 12.4 mg (7.34 μmol, 73%).

^{1}H NMR (CD_2Cl_2, 500 MHz): δ 8.00 (t, $^3J_{HH}$ = 7.9, 1H, 4-py), 7.71−7.74 (m, 9H, Ar^F + 3′-biph), 7.65−7.68 (m, 3H, 3-py + 6-biph), 7.64 (dd, $^3J_{HH}$ = 7.8, $^4J_{HH}$ = 1.5, 1H, 3-biph), 7.56 (br, 4H, Ar^F), 7.18 (td, $^3J_{HH}$ = 7.5, $^4J_{HH}$ = 1.3, 1H, 4′-biph), 7.09 (t, $^3J_{HH}$ = 7.5, 1H, 4-biph), 6.95 (td, $^3J_{HH}$ = 7.4, $^4J_{HH}$ = 1.5, 1H, 5-biph), 6.88 (td, $^3J_{HH}$ = 7.4, $^4J_{HH}$ = 1.4, 1H, 5′-biph), 5.89 (dd, $^3J_{HH}$ = 7.5, $^4J_{HH}$ = 1.4, 1H, 6′-biph), 4.58 (dvt, $^2J_{HH}$ = 17.4, J_{PH} = 9.8, 2H, pyC$\underline{H}_2$′), 3.89 (dvt, $^2J_{HH}$ = 17.3, J_{PH} = 8.2, 2H, pyC$\underline{H}_2$), 2.70 (dvt, $^2J_{HH}$ = 15.1, J_{PH} = 5.4, 2H, C$\underline{H}_2t$Bu), 2.31 (dvt, $^2J_{HH}$ = 15.2, J_{PH} = 6.2, 2H, C$\underline{H}_2t$Bu), 1.37 (dvt, $^2J_{HH}$ = 16.1, J_{PH} = 6.4, 2H, C$\underline{H}_2t$Bu′), 1.21 (dvt, $^2J_{HH}$ = 15.9, J_{PH} = 7.6, 2H, C$\underline{H}_2t$Bu′), 1.00 (s, 18H, tBu), 0.69 (s, 18H, tBu′).

^{13}C{^{1}H} NMR (CD_2Cl_2, 126 MHz): δ 177.5 (t, $^2J_{PC}$ = 7, CO), 162.2 (q, $^1J_{CB}$ = 50, Ar^F), 161.1 (vt, J_{PC} = 4, 2-py), 154.8 (br, 2′-biph), 152.9 (t, $^2J_{PC}$ = 10, 1′-biph), 151.3 (s, 2-biph), 141.0 (s, 4-py), 138.6 (s, 6-biph), 135.2 (br, Ar^F), 134.5 (t, $^2J_{PC}$ = 6, 1-biph), 131.8 (t, $^3J_{PC}$ = 2, 6′-biph), 129.3 (qq, $^2J_{FC}$ = 32, $^3J_{CB}$ = 3, Ar^F), 128.2 (s, 5-biph), 127.8 (s, 5′-biph), 126.4 (s, 4′-biph), 125.0 (q, $^1J_{FC}$ = 272, CF_3), 124.5 (s, 4-biph), 123.5 (vt, J_{PC} = 10, 3-py), 123.2 (s, 3′-biph), 122.5 (s, 3-biph), 117.9 (sept, $^3J_{FC}$ = 4, p-Ar^F), 45.3 (vt, J_{PC} = 29, py$\underline{C}H_2$), 44.0 (vt, J_{PC} = 26, $\underline{C}H_2t$Bu), 33.0 (vt, J_{PC} = 7, tBu{C}), 32.6 (vt, J_{PC} = 2, tBu′{C}), 32.5 (vt, J_{PC} = 25, $\underline{C}H_2t$Bu′), 32.2 (vt, J_{PC} = 6, tBu{CH_3}), 31.8 (vt, J_{PC} = 6, tBu′{CH_3}).

^{31}P{^{1}H} NMR (CD_2Cl_2, 162 MHz): δ −7.1 (s).

IR (CH_2Cl_2): ν(CO) = 2027 cm^{-1}. **ATR-IR**: ν(CO) = 2028 cm^{-1}.

HR ESI-MS (positive ion, 4 kV): 824.3691 ([M]$^+$, calcd 824.3698) m/z.

Anal. Calcd for $C_{72}H_{71}BF_{24}IrNOP_2$ (1687.30 g mol^{-1}): C, 51.25; H, 4.24; N, 0.83; found: C, 51.10; H, 4.10; N, 0.82.

4.12. Crystallography. Data were collected on a Rigaku Oxford Diffraction SuperNova AtlasS2 CCD diffractometer using graphite monochromated Cu Kα radiation and an Oxford Cryosystems N-HeliX cryostat (150 K for all complexes with additional collections at 50 and 100 K for **3** and **4**). Data were collected and reduced using CrysAlisPro.[28] The structures were solved using SHELXT and refined using SHELXL through the Olex2 interface.[29,30] All nonhydrogen atoms were refined anisotropically. Except for the hydride ligand in **7**, hydrogen atoms were placed in calculated positions and refined using the riding model. Full details for all structures reported are documented in the CIF, which have been deposited with the Cambridge Crystallographic Data Centre under CCDC 2327903−2327913.

4.13. Computational Details. Density functional theory calculations were carried out using the ORCA 5.0.3 program,[31] employing Goerigk's dispersion corrected ωB97X-D4 functional with the def2-TZVP basis set on all atoms and the associated def2-ECP effective core potential on Rh and Ir.[20] The RIJCOSX approximation was used to reduce the computational cost of calculations using the def2/J auxiliary basis set and integration grids set to DefGrid3.[32] All stationary points were verified to be minima (zero imaginary frequency) by frequency analysis at the same level of theory. NBO analyses were carried out using NBO 6.0.[21]

■ ASSOCIATED CONTENT

Supporting Information

The Supporting Information is available free of charge at https://pubs.acs.org/doi/10.1021/acs.organomet.4c00081.

NMR, IR, and ESI-MS spectra of complexes and selected reactions; further details on how the structural dynamics of **3** and **4** was modeled in solution, including Figure S50; further computational details, data, and analysis (PDF)

Optimized geometries of species examined computationally (XYZ)

Accession Codes

CCDC 2327903−2327913 contain the supplementary crystallographic data for this paper. These data can be obtained free of charge via www.ccdc.cam.ac.uk/data_request/cif, by emailing data_request@ccdc.cam.ac.uk, or by contacting The Cambridge Crystallographic Data Centre, 12 Union Road, Cambridge CB2 1EZ, UK; fax: +44 1223 336033.

■ AUTHOR INFORMATION

Corresponding Authors

Baptiste Leforestier − *Department of Organic Chemistry, University of Geneva, 1211 Geneva, Switzerland;* orcid.org/0000-0001-8547-6021; Email: baptiste.leforestier@unige.ch

Adrian B. Chaplin − *Department of Chemistry, University of Warwick, Coventry CV4 7AL, U.K.;* orcid.org/0000-0003-4286-8791; Email: a.b.chaplin@warwick.ac.uk

Authors

Jennifer E. Smart − *Department of Chemistry, University of Warwick, Coventry CV4 7AL, U.K.*

Ivan Prokes − *Department of Chemistry, University of Warwick, Coventry CV4 7AL, U.K.*

Complete contact information is available at: https://pubs.acs.org/10.1021/acs.organomet.4c00081

Notes

The authors declare no competing financial interest.

■ ACKNOWLEDGMENTS

We thank the Royal Society (RGF\EA\180128, J.E.S.; UF100592, UF150675; A.B.C.) for financial support. High-resolution mass-spectrometry data were collected using instruments purchased through the support from Advantage West Midlands and the European Regional Development Fund. Crystallographic data were collected using an instrument that received funding from the ERC under the European Union's Horizon 2020 research and innovation programme (grant agreement no. 637313). We thank Dr Amalia I. Poblador-

Bahamonde and the University of Geneva for the access to the "Yggdrasil" HPC cluster to perform the theoretical calculations.

REFERENCES

(1) Selected reviews: (a) Shilov, A. E.; Shul'pin, G. B. Activation of C−H Bonds by Metal Complexes. *Chem. Rev.* **1997**, *97*, 2879−2932. (b) Labinger, J. A.; Bercaw, J. E. Understanding and Exploiting C−H Bond Activation. *Nature* **2002**, *417*, 507−514. (c) Jones, W. D. Advances in Carbon−Hydrogen Activation. In *Comprehensive Organometallic*; Chemistry, I. I. I.; Mingos, D. M. P.; Crabtree, R. H., Eds.; Elsevier, 2007; Vol. *1*, pp 699−723. (d) Hartwig, J. F. Evolution of C−H Bond Functionalization from Methane to Methodology. *J. Am. Chem. Soc.* **2016**, *138*, 2−24. (e) Goldberg, K. I.; Goldman, A. S. Large-Scale Selective Functionalization of Alkanes. *Acc. Chem. Res.* **2017**, *50*, 620−626. (f) Crabtree, R. H.; Lei, A. Introduction: CH Activation. *Chem. Rev.* **2017**, *117*, 8481−8482. (g) Altus, K. M.; Love, J. A. The Continuum of Carbon−Hydrogen (C−H) Activation Mechanisms and Terminology. *Commun. Chem.* **2021**, *4*, No. 173.

(2) (a) Crabtree, R. H.; Holt, E. M.; Lavin, M.; Morehouse, S. M. Inter- vs. Intramolecular C−H Activation: A C−H−Ir Bridge in $[IrH_2(8\text{-methylquinoline})L_2]BF_4$ and a C−H + M → C−M−H Reaction Trajectory. *Inorg. Chem.* **1985**, *24*, 1986−1992. (b) Bengali, A. A.; Schultz, R. H.; Moore, C. B.; Bergman, R. G. Activation of the C−H Bonds in Neopentane and Neopentane-d_{12} by $(\eta^5\text{-}C_5(CH_3)_5)Rh(CO)_2$: Spectroscopic and Temporal Resolution of Rhodium-Krypton and Rhodium-Alkane Complex Intermediates. *J. Am. Chem. Soc.* **1994**, *116*, 9585−9589. (c) Bromberg, S. E.; Yang, H.; Asplund, M. C.; Lian, T.; McNamara, B. K.; Kotz, K. T.; Yeston, J. S.; Wilkens, M.; Frei, H.; Bergman, R. G.; Harris, C. B. The Mechanism of a C−H Bond Activation Reaction in Room-Temperature Alkane Solution. *Science* **1997**, *278*, 260−263. (d) Jay, R. M.; Banerjee, A.; Leitner, T.; Wang, R.-P.; Harich, J.; Stefanuik, R.; Wikmark, H.; Coates, M. R.; Beale, E. V.; Kabanova, V.; Kahraman, A.; Wach, A.; Ozerov, D.; Arrell, C.; Johnson, P. J. M.; Borca, C. N.; Cirelli, C.; Bacellar, C.; Milne, C.; Huse, N.; Smolentsev, G.; Huthwelker, T.; Odelius, M.; Wernet, P. Tracking C−H Activation with Orbital Resolution. *Science* **2023**, *380*, 955−960.

(3) Brookhart, M.; Green, M. L. H.; Parkin, G. Agostic Interactions in Transition Metal Compounds. *Proc. Natl. Acad. Sci. U.S.A.* **2007**, *104*, 6908−6914.

(4) Reviews and recent, illustrative examples: (a) Hall, C.; Perutz, R. N. Transition Metal Alkane Complexes. *Chem. Rev.* **1996**, *96*, 3125−3146. (b) Geftakis, S.; Ball, G. E. Direct Observation of a Transition Metal Alkane Complex, $CpRe(CO)_2$(cyclopentane), Using NMR Spectroscopy. *J. Am. Chem. Soc.* **1998**, *120*, 9953−9954. (c) Bernskoetter, W. H.; Schauer, C. K.; Goldberg, K. I.; Brookhart, M. Characterization of a Rhodium(I) σ-Methane Complex in Solution. *Science* **2009**, *326*, 553−556. (d) Pike, S. D.; Thompson, A. L.; Algarra, A. G.; Apperley, D. C.; Macgregor, S. A.; Weller, A. S. Synthesis and Characterization of a Rhodium(I) σ-Alkane Complex in the Solid State. *Science* **2012**, *337*, 1648−1651. (e) Young, R. D. Characterisation of Alkane σ-Complexes. *Chem. - Eur. J.* **2014**, *20*, 12704−12718. (f) Pike, S. D.; Chadwick, F. M.; Rees, N. H.; Scott, M. P.; Weller, A. S.; Krämer, T.; Macgregor, S. A. Solid-State Synthesis and Characterization of σ-Alkane Complexes, $[Rh(L_2)(\eta^2,\eta^2\text{-}C_7H_{12})][BAr^F_4]$ (L_2 = Bidentate Chelating Phosphine). *J. Am. Chem. Soc.* **2015**, *137*, 820−833. (g) Chadwick, F. M.; Rees, N. H.; Weller, A. S.; Krämer, T.; Iannuzzi, M.; Macgregor, S. A. A Rhodium−Pentane Sigma-Alkane Complex: Characterization in the Solid State by Experimental and Computational Techniques. *Angew. Chem., Int. Ed.* **2016**, *55*, 3677−3681. (h) Yau, H. M.; McKay, A. I.; Hesse, H.; Xu, R.; He, M.; Holt, C. E.; Ball, G. E. Observation of Cationic Transition Metal−Alkane Complexes with Moderate Stability in Hydrofluorocarbon Solution. *J. Am. Chem. Soc.* **2016**, *138*, 281−288. (i) Young, R. D. Alkane σ-Complexes. In *Comprehensive Organometallic Chemistry IV*; Parkin, G.; Meyer, K.; O'hare, D., Eds.; 2022; pp 502−520. (i) Watson, J. D.; Field, L. D.; Ball, G. E. $[Fp(CH_4)]^+$, $[\eta^5\text{-}CpRu(CO)_2(CH_4)]^+$, and $[\eta^5\text{-}CpOs(CO)_2(CH_4)]^+$: A Complete Set of Group 8 Metal−Methane Complexes. *J. Am. Chem. Soc.* **2022**, *144*, 17622−17629.

(5) Selected examples: (a) Hay-Motherwell, R. S.; Hussain-Bates, B.; Hursthouse, M. B.; Wilkinson, G. Synthesis and X -Ray Crystal Structure of Trimesitylrhodium(III). *J. Chem. Soc., Chem. Commun.* **1990**, 1242−1243. (b) Hay-Motherwell, R. S.; Wilkinson, G.; Hussain-Bates, B.; Hursthouse, M. B. Homoleptic Mesityls of Iridium(III,IV,V) and Ruthenium(IV,V). *J. Chem. Soc., Dalton Trans.* **1992**, 3477−3482. (c) Cooper, A. C.; Streib, W. E.; Eisenstein, O.; Caulton, K. G. Tert-Butyl Is Superior to Phenyl as an Agostic Donor to 14-Electron Ir(III). *J. Am. Chem. Soc.* **1997**, *119*, 9069−9070. (d) Clot, E.; Eisenstein, O.; Dubé, T.; Faller, J. W.; Crabtree, R. H. Interplay of Weak Interactions: An Iridium(III) System with an Agostic *tert*-Butyl but a Nonagostic Isopropyl Group. *Organometallics* **2002**, *21*, 575−580. (e) Scott, N. M.; Pons, V.; Stevens, E. D.; Heinekey, D. M.; Nolan, S. P. An Electron-Deficient Iridium(III) Dihydride Complex Capable of Intramolecular C−H Activation. *Angew. Chem., Int. Ed.* **2005**, *44*, 2512−2515. (f) Scott, N. M.; Dorta, R.; Stevens, E. D.; Correa, A.; Cavallo, L.; Nolan, S. P. Interaction of a Bulky N-Heterocyclic Carbene Ligand with Rh(I) and Ir(I). Double C−H Activation and Isolation of Bare 14-Electron Rh(III) and Ir(III) Complexes. *J. Am. Chem. Soc.* **2005**, *127*, 3516−3526. (g) Brayshaw, S. K.; Green, J. C.; Kociok-Köhn, G.; Sceats, E. L.; Weller, A. S. A Rhodium Complex with One Rh···C−C and One Rh···H−C Agostic Bond. *Angew. Chem., Int. Ed.* **2006**, *45*, 452−456. (h) Brayshaw, S. K.; Sceats, E. L.; Green, J. C.; Weller, A. S. C−C σ Complexes of Rhodium. *Proc. Natl. Acad. Sci. U.S.A.* **2007**, *104*, 6921−6926. (i) Douglas, T. M.; Chaplin, A. B.; Weller, A. S. Dihydrogen Loss from a 14-Electron Rhodium(III) Bis-Phosphine Dihydride To Give a Rhodium(I) Complex That Undergoes Oxidative Addition with Aryl Chlorides. *Organometallics* **2008**, *27*, 2918−2921. (j) Chaplin, A. B.; Green, J. C.; Weller, A. S. C−C Activation in the Solid State in an Organometallic σ-Complex. *J. Am. Chem. Soc.* **2011**, *133*, 13162−13168. (k) Phillips, N.; Rowles, J.; Kelly, M. J.; Riddlestone, I.; Rees, N. H.; Dervisi, A.; Fallis, I. A.; Aldridge, S. Sterically Encumbered Iridium Bis(N-Heterocyclic carbene) Complexes: Air-Stable 14-Electron Cations and Facile Degenerate C−H Activation. *Organometallics* **2012**, *31*, 8075−8078. (l) Tang, C. Y.; Phillips, N.; Kelly, M. J.; Aldridge, S. Hydrogen Shuttling: Synthesis and Reactivity of a 14-Electron Iridium Complex Featuring a Bis(alkyl) Tethered N-Heterocyclic Carbene Ligand. *Chem. Commun.* **2012**, *48*, 11999−12001. (m) Chaplin, A. B.; Weller, A. S. The Influence of Phosphine Cone Angle on the Synthesis and Structures of $[Rh(PR_3)(Binor\text{−}S)]^+$ Complexes That Show C−C Sigma Interactions. *J. Organomet. Chem.* **2013**, *730*, 90−94. (n) Jia, X.; Zhang, L.; Qin, C.; Leng, X.; Huang, Z. Iridium Complexes of New NCP Pincer Ligands: Catalytic Alkane Dehydrogenation and Alkene Isomerization. *Chem. Commun.* **2014**, *50*, 11056−11059. (o) Wang, Y.; Qin, C.; Jia, X.; Leng, X.; Huang, Z. An Agostic Iridium Pincer Complex as a Highly Efficient and Selective Catalyst for Monoisomerization of 1-Alkenes to Trans-2-Alkenes. *Angew. Chem., Int. Ed* **2017**, *56*, 1614−1618. (p) Gu, S.; Chen, J.; Musgrave, C. B.; Gehman, Z. M.; Habgood, L. G.; Jia, X.; Dickie, D. A.; Goddard, W. A.; Gunnoe, T. B. Functionalization of Rh^{III}−Me Bonds: Use of "Capping Arene" Ligands to Facilitate Me−X Reductive Elimination. *Organometallics* **2021**, *40*, 1889−1906.

(6) Hood, T. M.; Leforestier, B.; Gyton, M. R.; Chaplin, A. B. Synthesis and Structural Dynamics of Five-Coordinate Rh(III) and Ir(III) PNP and PONOP Pincer Complexes. *Inorg. Chem.* **2019**, *58*, 7593−7601.

(7) Gyton, M. R.; Leforestier, B.; Chaplin, A. B. Rhodium(III) and Iridium(III) Complexes of a NHC-Based Macrocycle: Persistent Weak Agostic Interactions and Reactions with Dihydrogen. *Organometallics* **2018**, *37*, 3963−3971.

(8) (a) Chaplin, A. B.; Tonner, R.; Weller, A. S. Isolation of a Low-Coordinate Rhodium Phosphine Complex Formed by C−C Bond Activation of Biphenylene. *Organometallics* **2010**, *29*, 2710−2714. (b) Knighton, R. C.; Emerson-King, J.; Rourke, J. P.; Ohlin, C. A.; Chaplin, A. B. Solution, Solid-State, and Computational Analysis of Agostic Interactions in a Coherent Set of Low-Coordinate Rhodium(III) and Iridium(III) Complexes. *Chem. - Eur. J.* **2018**, *24*, 4927−4938.

(9) (a) Hood, T. M.; Gyton, M. R.; Chaplin, A. B. Synthesis and Rhodium Complexes of Macrocyclic PNP and PONOP Pincer Ligands.

https://doi.org/10.1021/acs.organomet.4c00081
Organometallics 2024, 43, 1143−1154

Dalton Trans. **2020**, *49*, 2077−2086. (b) Hood, T. M.; Chaplin, A. B. Synthesis and Reactivity of Iridium Complexes of a Macrocyclic PNP Pincer Ligand. *Dalton Trans.* **2021**, *50*, 2472−2482. (c) Hood, T. M. Synthesis and Organometallic Chemistry of Rhodium and Iridium Complexes of Macrocyclic PNP and PONOP Pincer Ligands. Ph.D. Dissertation , University of Warwick, 2021.

(10) (a) Laviska, D. A.; Guan, C.; Emge, T. J.; Wilklow-Marnell, M.; Brennessel, W. W.; Jones, W. D.; Krogh-Jespersen, K.; Goldman, A. S. Addition of C−C and C−H Bonds by Pincer-Iridium Complexes: A Combined Experimental and Computational Study. *Dalton Trans.* **2014**, *43*, 16354−16365. (b) Laviska, D. A.; Zhou, T.; Kumar, A.; Emge, T. J.; Krogh-Jespersen, K.; Goldman, A. S. Single and Double C−H Activation of Biphenyl or Phenanthrene. An Example of C−H Addition to Ir(III) More Facile than Addition to Ir(I). *Organometallics* **2016**, *35*, 1613−1623.

(11) Yano, T.; Moroe, Y.; Yamashita, M.; Nozaki, K. Neopentyl-Substituted PNP-Pincer Ligand: Complexation with Iridium to Form an Iridacycle via Alkyl C−H Activation. *Chem. Lett.* **2008**, *37*, 1300−1301.

(12) Parker, G. L.; Lau, S.; Leforestier, B.; Chaplin, A. B. Probing the Donor Properties of Pincer Ligands Using Rhodium Carbonyl Fragments: An Experimental and Computational Case Study. *Eur. J. Inorg. Chem.* **2019**, *2019*, 3791−3798.

(13) (a) Davidson, J. J.; DeMott, J. C.; Douvris, C.; Fafard, C. M.; Bhuvanesh, N.; Chen, C.-H.; Herbert, D. E.; Lee, C.-I.; McCulloch, B. J.; Foxman, B. M.; Ozerov, O. V. Comparison of the Electronic Properties of Diarylamido-Based PNZ Pincer Ligands: Redox Activity at the Ligand and Donor Ability Toward the Metal. *Inorg. Chem.* **2015**, *54*, 2916−2935. (b) Lapointe, S.; Duari, P.; Gessner, V. H. Probing the Donor Strength of Yldiide Ligands: Synthesis, Structure and Reactivity of Rhodium Complexes with a PC Ylide N Pincer Ligand. *Chem. Sci.* **2023**, *14*, 3816−3825.

(14) For information about the use of fluorobenzenes as solvents see: Pike, S. D.; Crimmin, M. R.; Chaplin, A. B. Organometallic Chemistry Using Partially Fluorinated Benzenes. *Chem. Commun.* **2017**, *53*, 3615−3633.

(15) Tolman, C. A. Steric Effects of Phosphorus Ligands in Organometallic Chemistry and Homogeneous Catalysis. *Chem. Rev.* **1977**, *77*, 313−348.

(16) (a) Lu, Z.; Jun, C.-H.; de Gala, S. R.; Sigalas, M. P.; Eisenstein, O.; Crabtree, R. H. Geometrically Distorted and Redox-Active Organometallic Iridium Complexes Containing Biphenyl-2,2'-diyl. *Organometallics* **1995**, *14*, 1168−1175. (b) Iverson, C. N.; Jones, W. D. Rhodium-Catalyzed Activation and Functionalization of the C−C Bond of Biphenylene. *Organometallics* **2001**, *20*, 5745−5750.

(17) Cordero, B.; Gómez, V.; Platero-Prats, A. E.; Revés, M.; Echeverría, J.; Cremades, E.; Barragán, F.; Alvarez, S. Covalent Radii Revisited. *Dalton Trans.* **2008**, 2832−2838 Noting that the covalent radius of iridium (1.41 Å) is only marginally smaller than rhodium (1.42 Å)..

(18) For an illustrative examples of detection of agostic interactions in late transition metal complexes by this method see: (a) Cooper, A. C.; Clot, E.; Huffman, J. C.; Streib, W. E.; Maseras, F.; Eisenstein, O.; Caulton, K. G. Computational and Experimental Test of Steric Influence on Agostic Interactions: A Homologous Series for Ir(III). *J. Am. Chem. Soc.* **1999**, *121*, 97−106. (b) Huang, D.; Streib, W. E.; Bollinger, J. C.; Caulton, K. G.; Winter, R. F.; Scheiring, T. 14-Electron Four-Coordinate Ru(II) Carbyl Complexes and Their Five-Coordinate Precursors: Synthesis, Double Agostic Interactions, and Reactivity. *J. Am. Chem. Soc.* **1999**, *121*, 8087−8097.

(19) gNMR (Adept Scientific, Herts, UK), v 4.1.2.

(20) (a) Najibi, A.; Goerigk, L. DFT-D4 counterparts of leading meta-generalized-gradientapproximation and hybrid density functionals for energeticsand geometries. *J. Comput. Chem.* **2020**, *41*, 2562−2572. (b) Caldeweyher, E.; Bannwarth, C.; Grimme, S. Extension of the D3 dispersion coefficient model. *J. Chem. Phys.* **2017**, *147*, No. 034112. (c) Caldeweyher, E.; Mewes, J.-M.; Ehlert, S.; Grimme, S. Extension and evaluation of the D4 London-dispersion model for periodic systems. *Phys. Chem. Chem. Phys.* **2020**, *22*, 8499−8512. (d) Weigend, F.; Ahlrichs, R. Balanced basis sets of split valence, triple zeta valence and quadruple zeta valence quality for H to Rn: Design and assessment of accuracy. *Phys. Chem. Chem. Phys.* **2005**, *7*, 3297−3305. (e) Andrae, D.; Häußermann, U.; Dolg, M.; Stoll, H.; Preuss, H. Energy-adjusted ab initio pseudopotentials for the second and third row transition elements. *Theor. Chim. Acta* **1990**, *77*, 123−141.

(21) Glendening, E. D.; Landis, C. R.; Weinhold, F. NBO 6.0: Natural Bond Orbital Analysis Program. *J. Comput. Chem.* **2013**, *34*, 1429−1437.

(22) We have previously demonstrated that low valent carbonyl derivatives are most suitable for gauging net donor strength. For instance, whilst the ν(CO) measured for [Ir(PNP-*t*Bu)(biph)(CO)][BAr^F_4] in CH_2Cl_2 is 2028 cm^{-1} and therefore − within the error of the experiment − equivalent to that of **11**, the value of ν(CO) measured for [Ir(PNP-*t*Bu)(CO)][BAr^F_4] (1977 cm^{-1}) is considerably red-shifted relative to **4** (1991 cm^{-1}). ref. 12.

(23) King, R. B.; Cloyd, J. C.; Reimann, R. H. Poly(Tertiary Phosphines and Arsines). XIII. Neopentyl Poly(Tertiary Phosphines). *J. Org. Chem.* **1976**, *41*, 972−977.

(24) Crisenza, G. E. M.; McCreanor, N. G.; Bower, J. F. Branch-Selective, Iridium-Catalyzed Hydroarylation of Monosubstituted Alkenes via a Cooperative Destabilization Strategy. *J. Am. Chem. Soc.* **2014**, *136*, 10258−10261.

(25) (a) Buschmann, W. E.; Miller, J. S.; Bowman-James, K.; Miller, C. N. Synthesis of $[M^{II}(NCMe)_6]^{2+}$ (M = V, Cr, Mn, Fe, Co, Ni) Salts of Tetra[3,5-bis(trifluoromethyl)phenyl]borate. *Inorg. Synth.* **2002**, *33*, 83−91. (b) Martínez-Martínez, A. J.; Weller, A. S. Solvent-Free Anhydrous Li^+, Na+ and K^+ Salts of $[B(3,5\text{-}(CF_3)_2C_6H_3)_4]^-$, $[BAr^F_4]^-$. Improved Synthesis and Solid-State Structures. *Dalton Trans.* **2019**, *48*, 3551−3554.

(26) van der Ent, A.; Onderdelinden, A. L.; Schunn, R. A. Chlorobis(Cyclooctene)Rhodium(I) and -Iridium(I) Complexes. *Inorg. Synth.* **1990**, *28*, 90−92.

(27) Pregosin, P. S. *NMR in Organometallic Chemistry*; Wiley, 2012; pp 251−254.

(28) *CrysAlisPro*; Rigaku Oxford Diffraction: Yarnton, UK.

(29) Sheldrick, G. M. SHELXT − Integrated Space-Group and Crystal-Structure Determination. *Acta Crystallogr.* **2015**, *71*, 3−8.

(30) Dolomanov, O. V.; Bourhis, L. J.; Gildea, R. J.; Howard, J. A. K.; Puschmann, H. OLEX2: A Complete Structure Solution, Refinement and Analysis Program. *J. Appl. Crystallogr.* **2009**, *42*, 339−341.

(31) Neese, F. Software Update: The ORCA Program System − Version 5.0. *Wiley Interdiscip. Rev.: Comput. Mol. Sci.* **2022**, *12*, No. e1606, No..

(32) Weigend, F. Accurate Coulomb-fitting basis sets for H to Rn. *Phys. Chem. Chem. Phys.* **2006**, *8*, 1057−1065.

https://doi.org/10.1021/acs.organomet.4c00081
Organometallics 2024, 43, 1143−1154